https://doi.org/10.1016/j.conbuildmat.2019.117681

Loading Rate Effect on Fracture Behavior of Fiber Reinforced High Strength Concrete Using a Semi-Circular Bending Test

Mehran Aziminezhad[1], Sahand Mardi[2], Pouria Hajikarimi[3], Fereidoon Moghadas Nejad[4] and Amir H. Gandomi[5,*] (Corresponding Author)

[1]M.Sc, Department of Civil Engineering, Imam Khomeini International University, Qazvin, Iran
Cell: +98-936-797-4644
E-mail: mehranaziminezhad@edu.ikiu.ac.ir

[2]M.Sc, Department of Civil Engineering, Qazvin Branch, Islamic Azad University, Qazvin, Iran
Cell: +98-936-957-6161
E-mail: s.mardi@qiau.ac.ir

[3]Assistant Professor, Department of Civil Engineering, Qazvin Branch, Islamic Azad University, Qazvin, Iran
Cell: +98-912-582-6234
E-mail: pouria.hajikarimi@gmail.com

[4]Professor, Department of Civil & Environmental Engineering, Amirkabir University of Technology (Tehran Polytechnic), Tehran, Iran
Cell: +98-912-159-6723
E-mail: moghadas@aut.ac.ir

[5]Professor, Faculty of Engineering and IT, University of Technology Sydney, Ultimo, Australia (Corresponding Author)
Tel: +61 2 95145081
E-mail: gandomi@uts.edu.au

Loading Rate Effect on Fracture Behavior of Fiber Reinforced High Strength Concrete Using a Semi-Circular Bending Test

Abstract

Adding different types of fiber is one of the most common ways to enhance high strength concrete's mechanical behavior. In this paper, the effect of the loading rate and different type of fibers including glass, polypropylene, and steel were studied using the semi-circular bending (SCB) test method. It was evaluated that the SCB test can be used as a rapid and simple method to measure fracture properties of fiber reinforced high strength concrete (HSC) including ductility, energy absorption, and loading capacity by considering the effect of the loading rate on the parameters mentioned above. Specimens with glass fibers showed the most ductile behavior among all specimens with different types of fiber. On the other hand, steel fibers provided higher strength and higher energy absorption among the specimens. While specimens with steel fibers are highly sensitive to the loading rate in terms of peak load, this effect is not significant for specimens with glass and polypropylene fibers.

Keywords*: high strength concrete, fiber reinforced concrete, semi-circular bending test, loading rate, ductility*

1. Introduction

Recently, there has been an increase in the use of high strength concrete (HSC) due to its higher capacity and modulus of elasticity [1,2]. However, the more brittle behavior of HSC has led to the use of different types of fiber to provide sufficient ductility and deflection for concrete structures [3-9]. Polypropylene, glass, and steel fibers are the most common fibers used to enhance HSC ductile behavior [3,5,7].

Similar to other typical concrete, the routine experimental tests for determining the mechanical behavior of HSC are compressive, tensile, and flexural tests. Several research projects have been devoted to investigating the effect of fibers on mechanical behavior of HSC. Afroughsabet and Ozbakkaloglu [3] investigated the effect of silica fume, steel, and polypropylene fibers on high-strength concrete. The silica fume enhanced all the mechanical behavior including matrix-aggregate bond and compressive strength. The increase in the content of steel and polypropylene fibers improved the mechanical behavior as well. It was reported that the fibers ability to restrain crack propagation resulted in better fracture performance in the flexural bending test. Meanwhile, substitution of steel fiber with polypropylene resulted in lower mechanical strength parameters such as compressive strength, splitting tensile strength, and flexural strength. Kamal et al. [10] conducted research on the behavior and strength of HSC beams containing different types of fiber including steel and polypropylene. They discovered that the steel fiber increases compressive strength more efficiently compared to polypropylene fiber. For specimens with a lower reinforcement ratio, steel fibers increased ultimate loads by 13% in the conventional four points bending test. The effect of steel fibers on beams without stirrup was more significant in terms of the rising trend of maximum load.

From the point of view of fracture properties, Arslan [11] showed that the use of glass fiber in concrete generally increased compressive, tensile, and flexural strength of standard specimens but the increase in compressive strength was not significant. However, those values decreased when fiber content became too high (3 kg/m^3). The use of hybrid fiber reinforced concrete, namely a combination of steel and polypropylene fractions, showed improvements in failure modes. It was shown by Li et al. [12] that width of crack is noticeably smaller for elements with hybrid fibers in comparison with cracks on regular FRC specimens. It stems from synergic effect that exists among fibers on flexural behavior of concrete. It is also known that the use of hybrid FRC enhances the pull-out behavior of fiber due to the anchorage effect. However, it was reported by Deng et al. [13] that in a concrete matrix with straight smooth steel fiber, there is less sensitivity in sliding frictional force when polypropylene fiber is added in comparison with sole effect of chemical adhesion of concrete.

For the polypropylene fiber, Wang et al. [14] discovered that the compressive strength did not improve significantly by the use of the polypropylene fiber, but the improvements for tensile and flexural strength were noticeable. The effects of steel fiber on fracture properties are more significant, noted Ren et al. [15], who showed that compressive, tensile, and flexural strength rose by adding steel fiber. An increase of fiber content also improved the fracture performance but did point out that compressive strength will remain almost unchanged after increasing steel fiber volume to more than 1% of the total mixture volume. This phenomenon was also pronounced by Li et al. [12]. Although compressive strength increases due to bridging effects, high elastic modulus and crack arresting of steel fibers, adding lots of fiber precipitate initial damages such as weak interfaces and voids. Damage evolution and hardening/softening constitutive laws are determinate parameters that solidly define specimen performance. As for FRC, it was investigated by Chi et al. [16] that defining constitutive laws based on fiber effect-dependent parameters, demonstrate failure mechanism of FRC with high accordance with experimental results under multiaxial and cyclic loadings, using modified concrete damaged plasticity model. This proves that mechanical performance and damage mechanism of FRC elements are highly associated with fiber characteristics.

Teng et al. [17] investigated flexural behavior of high-performance hybrid-fiber-reinforced concrete. In this study, maximum modulus of rupture belong to the FRC samples including only double hooked-end (DHE) steel fibers in comparison to FRC samples prepared with single hooked-end (HE) steel fibers or polyvinyl alcohol (PVA) fibers. This advantage can be related to the high elastic modulus, tensile strength, and effective anchoring mechanism of DHE steel fibers. For instance, DHE steel fibers can resist higher pull-out forces compared to those pull-out forces that could be resisted by HE steel fibers or straight PVA fibers.

According to Li et al. [18,19] studies, steel fiber considerably enhances the cyclic mechanical properties of concrete with regard to toughness, peak stress, peak strain, and post-peak ductility. Moreover, the capacity of steel fiber reinforced concrete (SFRC) in hysteretic energy dissipation was shown stronger than plain concrete. However, the elastic stiffness of SFRC is observed to decrease with increasing loading cycles.

By using acoustic emission (AE) technique, it was shown that response and destruction behavior of SFRC under cyclic tension were similar to specimens under the monotonic loading. Furthermore, the shear cracks and the AEs activity in concrete increase with an increase in fiber properties for both cyclic and monotonic loading cases. As proved by AE, the failure of SFRC mostly exhibits a shear cracking mode that is induced by fiber pull-out and fiber sliding proceedings. Fibers can restrain the sliding between the two parts of cracks and form a truss because of the dowel action.

Zhang et al. [20] investigated the notch effect on the behavior of concrete beams under three-point loading and indicated parameters that influence fracture performance. In the beams with a double notch, the location of each notch and aggregate distribution are key factors to determine the dead and live notch (a dead notch does not participate in crack propagation during the three-point loading test, but live notch does). When aggregate content is constant, only aggregate grading has an effect on post-elastic behavior. Therefore, in order to study the effect of notch and minimize errors when specimen is notched, aggregate content and grading play a major role. To evaluate of fiber effect on behavior of HSC, it is vital to recognize the function of fiber in a concrete matrix. When cracks start to spread, fibers resist the further propagation by enduring the tensile force and bridging two sides of concrete matrix according to the fiber-bridging constitutive law of composites [21]. The result is a residual strength in post-peak range by the strain hardening effect. Eventually, higher ductility and energy absorption will be achieved. Several parameters influence this performance including the fibers orientation and concrete matrix spalling at the fiber exit point where the latter is highly sensitive to the loading rate itself. Both parameters were studied by conducting a pull-out test between fibers and concrete matrix, and a few researchers [22] also considered the effect of the loading rate. It is noteworthy that very little of the research considered all these parameters in the HSC matrix, and it was mostly limited to steel fiber [23,24]. Tai and El-Tawil [24] conducted research on this matter, and the results proved that the straight smooth type was highly sensitive to the loading rate while hooked and twisted steel fibers were indicative of less stable trends and changed the loading rate. Specimens reinforced with straight smooth steel fibers experienced an increase in the energy absorption capacity as the loading rate increased.

Different responses of fibers in each test led researchers to develop and examine new methods of testing materials in order to achieve a better understanding of fiber reinforced concrete performance in different situations. A simple and rapid test method exists in pavement and asphalt design known as semi-circular bending (SCB) test, which can be applied in a similar way to concrete specimens. Fracture parameters of brittle materials such as rock and concrete also could be investigated by the SCB method [25].

The SCB test method was initially used in rock mechanics in order to investigate characteristics of this material [26-29]. Furthermore, it is a novel and standard test method in the context of asphalt technology science. Different property values such as the stress intensity factor (SIF), fatigue, tensile strength [30], crack opening, bending strength, energy dissipation, ductility, dynamic fracture toughness [31], and other similar factors can be obtained. The specimen failure in the SCB test method indicates that tension is the premier failure mode [30]. In order to minimize error in the results, cutting the semi-circular disk with a small notch and guide the crack in a prescribed direction is suggested. However, any minor inexactitude for making notch direction into load point might lead to some errors in the final results [32]. Gabriel Nsengiyumva [33] conducted extensive research on asphalt specimens with different thickness size, notch length, and loading rate. The effect of each variable was evaluated clearly and proved that the SCB method could be used as a rapid and simple method for investigating the influence of geometric and inherent properties on mechanical performance of specimens. The SCB test can be used as a method to analyse the energy dissipation. Sheng Tang [34] conducted research at Iowa State University and proved the SCB method's ability to investigate the specimens' behavior from an energy point of view. Energy is a product of force with a load-line movement distance. He also proved that when the material deforms under linear elastic conditions, notch length had no significant effect. When material enters the post-elastic state, notch length has a significant effect on specimen performance. Several researchers studied numerical modeling of the SCB test method by investigating the crack propagation by implementing the extended finite element method (XFEM). The results showed that the SCB test method could be easily modeled numerically, and it is well suited for modeling of discontinuous features such as inclusions and cracks [35,36].

This paper deals with the investigation of high strength concrete performance reinforced with different fibers using the SCB test method under different loading rates, in which tension is premier failure mode. Polypropylene, glass, and steel fibers were used in three different contents separately with 0.5%, 1% and 1.5% of concrete volume for each type of fiber. One specimen was also cast without fiber as a control sample. The experimental tests were conducted with different loading rates including 0.5, 1 and 5 mm/min. Afterward, the fiber effect on both rheological and mechanical performance of high strength concrete was evaluated. The load-displacement curves for each specimen were acquired by a hydraulic universal testing machine (UTM). By considering the effect of the loading rate, the variation of ductility, the peak load, the maximum displacement and energy absorption for each type of fiber have been studied and discussed in this research.

2. Materials and Test Methods

2.1. Materials

Commercial ASTM C150 Portland cement type II was used for the study. It was produced by Jovin Khorasan™ Company, located in Khorasan, Iran. Silica-fume as a pozzolanic material was applied to increase the strength of concrete. The chemical analysis of materials is shown in Table 1. A polycarboxylate ether superplasticizer was provided by Zhikava™ with a specific gravity of 1090 kg/m^3. The quartzite (micro-sand) aggregates were specified by using commercial codes of Iran Kansar™ Company including MR-150, R-101, and ZS-200. ZS-200 with a size smaller than 75 microns was used as filler. The grading diagram of aggregates is shown in Figure 1. The three types of fiber with 12.5 mm length, used in this study was acquired from Sirjan Nano Yarn and Granule™ Company, shown in Figure 2 with their mechanical and physical properties shown in Table 2.

2.2. Mixture design

The mixture design includes an 1100 kg/m^3 binder with a 20/80 silica fume-cement ratio. Aggregates are also involved with 65% MR-150, 10% R-101 and 25% ZS-200. A water-cement ratio was considered to be 0.18 and 3% superplasticizer by the weight of binder materials was added to the mixture.

Steel, glass, and polypropylene fibers were used individually by concrete volume of 0.5, 1, and 1.5%, respectively.

2.3. Sample Preparation

There were three steps taken for the mixing process: dry mix, wet mix, and adding fibers. For the first step, cement, silica-fume, and aggregates were mixed for 2 minutes. Afterward, water and superplasticizer were added to the spinning mixer gradually for 30 seconds. Five minutes after this wet mix, the last step was performed by adding fibers. This step continued for 2 minutes. Prepared concrete was used for a rheometer test. Then, a cylindrical mold with diameter of 150 mm and height of 300 mm was filled for a semi-circular bending (SCB) test. Cylindrical samples were kept in moist conditions for 1 day. Then samples were put in wet curing and kept there for 4 days at a temperature of 60 °C. They were evaluated by a trial and error process so that the specimens could reach their final strength after this period. A compressive strength of 105.2 MPa was recorded for a 100×100×100 mm cubic control sample in accordance with BS 1881-116 [37]. Cured cylindrical samples were cut at the top and bottom for a length of 50 mm. The middle part was cut into 8 circular slices with thicknesses of 25 mm. Each circular slice was also cut by an electric saw to obtain semi-circular specimens, as shown in Figure 3. Finally, by using a water-jet technology, a notch was made with a width of 3 mm and a height of 15 mm at the center of the specimens, depicted in Figure 4.

2.4. Rheometer

In this study, to evaluate the rheological behavior of concrete samples, yield stress was recorded according to stress growth tests [38]. A cylindrical container with a radius of 150 mm and a height of 300 mm was filled with concrete (Figure 5). For the stress growth test, a vane with a radius of 50 mm and a height of 100 mm was rotated with 1.5 rpm in the cylindrical container until declination of the torque-time graph appeared. The maximum torque corresponds to the yield stress calculated by Eq. (1), as follows:

$$\tau_0 = \frac{2H}{\pi D^3\left(\frac{H}{D} + \frac{1}{3}\right)} \tag{1}$$

where τ_0 is yield stress, T is maximum torque, D is diameter of vane, and H is the height of the vane.

2.5. Semi-Circular Bending (SCB) Test

Prepared SCB specimens with a thickness of 25 mm were tested for 0.5, 1 and 5 mm/min loading rates. The 0.5 mm/sec loading rate was chosen (because of a lower covariance value [29]) to study the effect of fiber types on mechanical behaviors, and later on, the effects of loading rates were considered. A 250 kN hydraulic universal testing machine (UTM) was used for applying load and recording force-displacement diagrams. For each diagram, two specimens were tested and averaged to increase the accuracy of the results. The SCB specimens were placed on the pinned supports with a 130 mm span as shown in Figure 4.

The crack propagation on the specimen's face was recorded by a high-resolution camera (Canon 60D).

3. Results and Discussion

3.1. Rheological Behavior

In order to evaluate the rheological behavior of concrete to determine yield stress in different types of fiber-reinforced high strength concrete, a rheometer was used. Figure 6 depicts the amount of yield stress (in the logarithmic scale). As it can be seen in this figure, adding glass and polypropylene to control the sample leading to increasing the yield stress while increasing the content of steel fiber had no effect on yield stress of fiber-reinforced concrete.

Fibers have a significant influence on rheological and mechanical properties of cementitious material, and their impact depends on parameters like the length, the diameter, the rigidity, and the volume fraction of fibers [39,40]. Fiber factor is well-known as a proper index to measure and control the workability and rheology of suspensions that contain fiber. The fiber factor is determined by multiplying volume fraction (φ) and aspect ratio (r). Fiber factors are tabulated in Table 3. The highest amount of fiber factor belongs to G 1.5% that has the highest yield stress. Increasing the volume fraction of fiber increases the contact and interaction between particles of fibers. After a certain limit, the fluidity of mortar decreases, and fibers resist the flow. Samples with fiber factors higher than F_d (a dense fiber factor) are not be able to flow. In Mehdipour's article [40], this amount (F_d) was reported to be 300 for PP. However, the report showed the F_d increased by decreasing the rigidity of fibers. It may be because the higher fiber friction needs more energy to achieve the same flowability. In this research, steel is known as a rigid fiber and glass and polypropylene are known as flexible fibers. However similar to Mehdipour's results [40], samples containing steel fiber were flowable and improved workability, while other samples containing glass and polypropylene resisted flow. Results of lower yield stress belong to specimens containing steel fiber with minor variations in the fiber. The low amount of fiber factor shows a lot of energy is not needed to spread steel fibers. However, by increasing suspension particles of glass and polypropylene fibers, the energy dissipation of fiber increases. The incremental amount of yield stress for these two fibers is indicative of this phenomenon.

3.2. Mechanical Behavior

Figure 7 shows force versus displacement of the SCB test for the control sample of concrete without fibers. As it can be seen in this figure, by increasing the displacement at a constant rate the associated force increases, and simultaneously, the crack mouth gradually opens until the peak of force reaches the point at which the prescribed crack starts to propagate at the tip of the U-notch. Figure 8 depicts this process for the control sample both before the crack propagation and after it, and also for a fiber-reinforced sample after propagating the prescribed crack. Based on Figure 7, it is apparent that the fracture behavior of the control sample is very brittle as it fails suddenly without any presence of ductility.

The brittle behavior of the control sample is expected because of the general properties of high strength concrete [41]. Meanwhile, using fibers with high tensile strength significantly alters fracture behavior of the concrete samples. These SCB test results are illustrated in Figure 9 to 11 for fiber-reinforced concrete (FRC) with glass, polypropylene, and steel fibers, respectively (with a constant loading rate of 0.5 mm/sec). In all the figures mentioned above, it is evident that the brittle behavior of the control sample was substituted by a ductile behavior with higher displacement and amount of force at the peak point and a greater amount of area under the curve of force-displacement.

Regarding Figures 9 to 11, typically by increasing the fiber content in concrete samples, the force at peak and the area under the curve of force-displacement increases, which shows more ductile behavior of fiber reinforced samples in comparison with the control and with each other with a lower amount of fibers. Table 3 shows the amount of these parameters for a constant loading rate of 0.5 mm/sec, including peak load, displacement at peak, maximum displacement, and second peak load. The second peak load is the quantity of the first local increase or smoothness of the force-displacement curve after the first peak load which reflects the individual performance of fibers in concrete.

According to Table 3, adding fibers to the control sample increased the peak load between 1.083 (0.5% of steel) and 1.758 (1.5% of steel) times more than the peak load of the control sample which showed a higher influence of steel fiber on load capacity when fiber amount was varied. Also, displacement at peak increases between 1.380 (0.5% of glass) and 2.394 (1.5% of glass) times more than displacement at peak of the control sample. In order to determine the maximum displacement of each sample, a rational criterion was considered for interrupting the SCB test in which the maximum displacement takes place at the force which loses 95% of the peak load quantity. By considering this criterion, the maximum displacement of fiber reinforced samples is in the range of 5.67 mm (0.5% of glass) to 12.06 mm (1.5% of glass), which is respectively, 22.051 and 46.837 times greater than the control sample and shows a wider range of displacement. Following this, three primary and meaningful parameters were calculated and discussed for all samples including ductility, the area under the force-displacement curve and the ratio of the second peak load to the first one. These parameters reflect the effect of adding fibers to the fracture behavior of the control sample.

3.3. Ductility

The ductility index of concrete samples can be defined as a ratio of maximum displacement to displacement at peak (the first peak load) as follows [42]:

$$ductility\ \ index = \frac{maximum\ \ displacement}{displacement\ \ at\ \ peak} \tag{2}$$

The maximum displacement was defined as displacement in which the response force decreases to 90% of the first peak load. According to Eq. (2), it is evident that by increasing the amount of maximum displacement and widening the range of displacement in comparison with displacement at peak, ductility will be enhanced. For a concrete sample, it is actually better to experience a higher amount of displacement at maximum force to start propagating the crack tip and then continue to carry a load for a larger quantity of displacement up to its maximum value.

Figure 12 depicts ductility of all fiber reinforced samples besides the control sample, which are calculated implementing Eq. (2) and data, are represented in Table 3. As it can be seen in Figure 12, there is a significant difference between the ductility of the control sample and the FRC ones. Fibers effectively increase concrete ductility from at least 10.392 (for 0.5% of steel) up to 19.556 (for 1.5% of glass) times greater than the control sample. Concrete which is reinforced with 1.5% of glass fibers has the superior ductility among all FRC samples, and the sample with 0.5% of steel has the lowest. Adding fibers increases the tensile strength of concrete because each fiber acts as a small tensile element in its local effective zone and avoids a failure of concrete in this zone. Thus, by increasing the displacement in the SCB test and increasing tensile stress due to bending, fibers start to actively interact with concrete to resist against tensile stress up to their maximum failure tensile strength.

By increasing the fiber content, ductility enhances which can apparently be seen for glass fibers with a linear trend of ductility versus fiber content. However, it can be seen that there is no difference between 1 and 1.5% of PP fibers due to similar ductility ratios.

3.4. Stored and Released Energy

During a fracture test like the SCB test, by passing time and increasing the amount of strain, energy can be stored up to peak load when cracks start to propagate at its tip. After that, the stored energy can be released by opening the crack and moving its tip forward. The summation of stored and released energy can be determined by calculating area under force-displacement curve. This quantity of area under the curve is considered as a performance index of FRC. Figure 13 shows area under a force-displacement curve for all samples. As it can be seen in this figure, this quantity increases by increasing the fiber content for all FRCs. The highest value was captured for 1.5% of steel fiber (31.93 times greater than control sample) and the lowest one was related to 0.5% of PP (7.57 times greater than control sample). It is evident that there is a meaningful difference between the control sample and the FRCs, which proves the effect of fiber on increasing stored and released energy of samples. Actually, the main reason for increasing the summation of stored and released energy of the FRCs in comparison with the control sample is enhancing peak load (related to stored energy) and widening the range of applicable displacement (related to releasing energy) after a crack rupture.

3.5. Second Peak Load

During the running of the SCB test, a remarkable phenomenon was captured for all fiber reinforced samples [43]. It is well-known that, generally, when the peak load is achieved, by increasing the displacement and passing time, force is reduced as in Figure 7 for the control sample. The process of force reduction for the FRCs is slower than that of the control sample because of the higher ductility. This can be seen in Figure 9 to 11. After reaching the peak load there is another peak or smoothening zone that was unexpected and directly related to using fiber. This phenomenon was also reported in a three-point bending beam test by ASTM C1609 [44], which shows the SCB test method's ability to exhibit all details during the test precisely. After rupturing the U-notched crack and starting propagation on its tip by increasing the crack mouth opening, fibers find a way to thoroughly use their tensile strength potential. Therefore, a second peak load can be captured, such as 0.5% or 1% of glass (Figure 9) and 1.5% of PP (Figure 10) or a smooth zone like 0.5% of PP (Figure 10) or 0.5% of steel (Figure 11).

The higher amount of the second peak load or smooth zone could reflect the better fracture performance of the FRC samples. Thus, a simple index is defined that shows the ratio of the amount of second peak load or smooth zone to the first peak load as follows:

$$Ratio\ of\ \ Peak\ \ Loads = \frac{Second\ \ Peak\ \ Load\ \ or\ \ Smooth\ \ Zone}{First\ \ Peak\ \ Load} \qquad (3)$$

Figure 14 shows this ratio for all FRC samples. It is apparent that there is no value for the control sample because there is no second peak load or smooth zone. The highest peak load ratio is for a sample containing steel fibers, which is approximately 100% for using 1.5% of steel fibers. The lower ratio is related to PP fibers. Results have shown that by increasing the fiber content in FRCs, an increasing trend can be seen for all FRCs.

3.6. The Effect of Loading Rate

Figures 15 to 17 demonstrate force versus displacement of the SCB test at different loading rates (0.5, 1 and 5 mm/min) for various volumes of polypropylene, glass, and steel fibers.

In general, loading rate growth resulted in a considerable rise of peak loads for all different types of fiber. According to Figure 18, the maximum load capacity belongs to 1.5% ST in all loading rates. Polypropylene and glass fibers have a slight influence on changes in peak load due to loading rate variation, while steel fiber is highly sensitive to loading rates in comparison with glass and polypropylene, as demonstrated in Figure 18. This procedure is reasonable, taking the failure mode of fibers in concrete into consideration. It has been proved in another test method, namely in a fiber pull-out test for a normal strength matrix undertaken by Gokoz and Naaman [45] that glass and polypropylene fibers tend to fail, mostly when they are under tension load, independent of load velocity and matrix. However, steel fibers tend to pull out of a concrete matrix when the loading rate is determinative to assess fiber condition while coming out of the concrete matrix. This phenomenon arises from the solid structure of steel fiber, while the glass and polypropylene fibers are easily deformed. Therefore, the effect of the loading rate is slighter in comparison with steel fiber. In this research, the high strength concrete is used, and stronger bond strength between fibers and the concrete matrix is expected as well as a higher sensitivity to the loading rate. The failure in bond strength begins through interfacial debonding between concrete and fiber, which continues until the whole embedment length of the fiber comes out of the concrete [46].

The range of changes in peak load for polypropylene and glass are 15% and 14%, respectively. Consequently, the changes in the peak load for steel fiber are about 30%. Smooth shaped steel fiber is highly rate-sensitive, as it reported in other research as well, and the loading rate has a direct influence on obtained peak load value [47].

The area under the curve represents the specimen's ability to store and release energy, and it considers the effect of either maximum loading capacity or maximum displacement. Figure 19 shows the area under the curve for different loading rates. For all types of fiber, the area under curve did not experience any remarkable change between 0.5 and 1 mm/min and energy absorption ability is nearly constant. However, increasing the loading rate to 5 mm/min results in a significant increase in the area under the curve for all types of fiber. Steel fiber experienced the maximum increase in its energy absorption ability by increasing the loading rate to 5 mm/min. The dissimilar pull-out behavior of tension in different fibers is the main reason for the different responses under various loading rates. The pull-out behavior itself is under the influence of bond mechanisms between fiber and concrete matrix, as it has been reported in past research [48,49].

To consider the bond mechanism behavior in more detail, it should be noted that fibers resist pull-out loads by elastic shear bond and fiber bearing, also known as adhesion and anchorage, respectively. However, the elastic shear bond has slight effect while bearing plays a major role to resist the load before reaching the failure point, because that maximum strain provided by elastic shear bond is very slight and would reach its peak as soon as pull-out behavior begins. However, the fibers' bearing is more influential, rooting in basic fiber characteristics such as aspect ratio and tensile strength. Considering the fact that the strength of the bond stem from matrix is identical for all specimens, the two aforementioned parameters are determining the mechanism behavior. Once the elastic shear bond decays, the anchorage process starts by developing a deformed zone around the fiber within the matrix, and it continues until the load in fiber reaches the yield strength. This is when fibers experience local deformations. This also comes with the possible failure of the matrix, depending on the tensile strain capacity in which matrix splitting take place. This phenomenon was seen in specimens with steel fibers that have more tensile strength with considerable aspect ratio. Some of fibers were pulled out of the matrix without reaching their ultimate failure strength, and this was more noticeable for specimens with higher steel content. It should be taken into account that constitutive steel behaviors, such as strain hardening characteristics and post-hardening strength, are also affecting the pull-out behavior of steel fibers, whereas the polypropylene and glass fibers do not have such constitutive characteristics that would significantly affect the behavior when they reach their yield strength.

Figure 20 illustrated the ratio of second peak load to the first peak load, which represents the definition of residual strength of the specimen after reaching its maximum loading capacity. Steel fibers with 5 mm/min loading rate experience most residual strength (higher first peak load to second peak load) and changes in steel fiber percentage did not influence the ratio of peak loads remarkably. This is because of the immediate reaction of steel fibers at higher loading rates and its solid structure while polypropylene and glass fibers need the specimen crack to become wider and resist the tensile force. This delay results in descent in the load-displacement diagram. Therefore, the ratio of peak loads for polypropylene and glass fiber is lower compared to steel fiber. This procedure can be observed by studying the fiber effect and loading rate effect on the ratio of peak loads as well. The maximum effect of the loading rate in the ratio of peak loads for polypropylene and glass fiber is 15% and 52%, respectively;

However, the effect of an increase in fiber content for polypropylene and glass fiber is 172% and 283%, respectively.

4. Conclusions

In this research, polypropylene, steel, and glass fibers were used in high strength concrete samples with three percentages of 0.5, 1 and 1.5% by volume of concrete. In the fresh phase, rheological behavior of samples was assessed by the stress growth test method, and in the hardening phase, the mechanical behavior of FRC samples was investigated according to a SCB test as a novel method for evaluating the HSC specimen's properties. The SCB test is a simple and rapid test method, which requires an extremely low amount of materials to be examined, and samples that can be fabricated in a short time. The main results can be summarized as follows:

- In the fresh phase, by increasing PP and glass fiber volume fraction, the rheological yield stress of the fresh concrete increased whereas this parameter was constant for samples with steel fiber. The sample with volume fraction of 1.5% glass has highest yield stress.
- The SCB test showed the ability for evaluating all basic fracture properties of the HSC specimens similar to bending beam test, including the trivial effects of fiber type, fiber amount, and loading rate on ductility, energy absorption capacity, maximum loading capacity, observation of second peak load, and smoothing zone in the post-elastic range.

- The 1.5% ST specimen had approximately 100% ratio of peak loads, indicating an immediate tensile reaction of steel fibers after opening crack mouth. On the other hand, glass and polypropylene fibers need the crack to become wide enough to participate in providing the residual strength because of their basic deformable structure. This phenomenon was easily observed during the SCB test for different types of fiber.
- Although specimens reinforced with steel fibers had higher loading capacity and energy absorption, specimens with glass fibers showed more ductile performance. This is directly related to the type of fiber and its behavior.
- Polypropylene and glass fiber have a slight influence on changes in peak load by loading rate variation. Steel fiber is highly sensitive to the loading rate, which is similar to fiber pull-out and beam bending test results reported in the literature.

6. References

[1] ACI Committee 363 Report on High-Strength Concrete. ACI 363R-10, American Concrete Institute Committee 363, Farmington Hills, MI. 2010.

[2] S. Mardi and M. Bastami, Developing a Cost-Effective Approach for Enhancing the Rheological and Mechanical Behavior of High Strength Self-Compacting Concrete, J. Struct. Eng. Geo-Tech. 8(1) (2018) 41-54.

[3] V. Afroughsabet and T. Ozbakkaloglu, Mechanical and durability properties of high-strength concrete containing steel and polypropylene fibers, Constr. Build. Mater. 94 (2015) 73–82.

[4] H. Ueno, M. Beppu, and A. Ogawa, A method for evaluating the local failure of short polypropylene fiber-reinforced concrete plates subjected to high-velocity impact with a steel projectile, Int. J. Impact Eng. 105 (2017) 68-79.

[5] A. Caggiano, S. Gambarelli, E. Martinelli, N. Nisticò, and M. Pepe, Experimental characterization of the post-cracking response in Hybrid Steel/Polypropylene Fiber-Reinforced Concrete, Constr. Build. Mater. 125 (2016) 1035-1043.

[6] J.-H. Lee, B. Cho, E. Choi, and Y.-H. Kim, Experimental study of the reinforcement effect of macro-type high strength polypropylene on the flexural capacity of concrete, Constr. Build. Mater. 126 (2016) 967-975.

[7] M. K. Yew, H. B. Mahmud, B. C. Ang, and M. C. Yew, Influence of different types of polypropylene fibre on the mechanical properties of high-strength oil palm shell lightweight concrete, Constr. Build. Mater. 90 (2015) 36-43.

[8] N. Yermak, P. Pliya, A.-L. Beaucour, A. Simon, and A. Noumowé, Influence of steel and/or polypropylene fibres on the behaviour of concrete at high temperature: Spalling, transfer and mechanical properties, Constr. Build. Mater. 132 (2017) 240-250.

[9] J. M. Yang, H. O. Shin, and D. Y. Yoo, Benefits of using amorphous metallic fibers in concrete pavement for long-term performance, Arch. Civ. Mech. Eng. 17 (2017) 750-760.

[10] M. M. Kamal, M. A. Safan, Z. A. Etman, and R. A. Salama, Behavior and strength of beams cast with ultra high strength concrete containing different types of fibers, HBRC J. 10 (2014) 55-63.

[11] M. E. Arslan, Effects of basalt and glass chopped fibers addition on fracture energy and mechanical properties of ordinary concrete: CMOD measurement, Constr. Build. Mater. 114 (2016) 383-391.

[12] B. Li, Y. Chi, L. Xu, Y. Shi, C. Li, Experimental investigation on the flexural behavior of steel-polypropylene hybrid fiber reinforced concrete, Constr. Build. Mater. 191 (2018) 80–94. https://doi.org/10.1016/j.conbuildmat.2018.09.202.

[13] F. Deng, X. Ding, Y. Chi, L. Xu, L. Wang, The pull-out behavior of straight and hooked-end steel fiber from hybrid fiber reinforced cementitious composite: Experimental study and analytical modelling, Compos. Struct. 206 (2018) 693–712. https://doi.org/10.1016/j.compstruct.2018.08.066.

[14] D. Wang, Y. Ju, H. Shen, L. Xu, Mechanical properties of high performance concrete reinforced with basalt fiber and polypropylene fiber, Constr. Build. Mater. 197 (2019) 464–473. https://doi.org/10.1016/j.conbuildmat.2018.11.181.

[15] G.M. Ren, H. Wu, Q. Fang, J.Z. Liu, Effects of steel fiber content and type on static mechanical properties of UHPCC, Constr. Build. Mater. 163 (2018) 826–839.

[16] Y. Chi, M. Yu, L. Huang, L. Xu, Finite element modeling of steel-polypropylene hybrid fiber reinforced concrete using modified concrete damaged plasticity, Eng. Struct. 148 (2017) 23–35. https://doi.org/10.1016/j.engstruct.2017.06.039.

[17] S. Teng, V. Afroughsabet, C.P. Ostertag, Flexural behavior and durability properties of high performance hybrid-fiber-reinforced concrete, Constr. Build. Mater. 182 (2018) 504–515. https://doi.org/10.1016/j.conbuildmat.2018.06.158.

[18] B. Li, L. Xu, Y. Chi, B. Huang, C. Li, Experimental investigation on the stress-strain behavior of steel fiber reinforced concrete subjected to uniaxial cyclic compression, Constr. Build. Mater. 140 (2017) 109–118. https://doi.org/10.1016/j.conbuildmat.2017.02.094.

[19] B. Li, Y. Chi, L. Xu, C. Li, Y. Shi, Cyclic tensile behavior of SFRC: Experimental research and analytical model, Constr. Build. Mater. 190 (2018) 1236–1250. https://doi.org/10.1016/j.conbuildmat.2018.09.140.

[20] C. Zhang, X. Yang, H. Gao, and H. Zhu, Heterogeneous Fracture Simulation of Three-point Bending Plain-concrete Beam with Double Notches, Acta Mech. Solida Sin. 29(3) (2016) 232-244.

[21] B. Nematollahi, J. Sanjayan, J. Qiu, and E. H. Yang, High ductile behavior of a polyethylene fiber-reinforced one-part geopolymer composite: A micromechanics-based investigation, Arch. Civ. Mech. Eng. 17(3) (2017) 555-563.

[22] D. J. Kim, S. El-Tawil, and A. E. Naaman, Loading rate effect on pullout behavior of deformed steel fibers, ACI Mater. J. 105(6) (2008) 576-584.

[23] M. Xu, B. Hallinan, and K. Wille, Effect of loading rates on pullout behavior of high strength steel fibers embedded in ultra-high performance concrete, Cem. Concr. Compos. 70 (2016) 98-109.

[24] Y.-S. Tai and S. El-Tawil, High loading-rate pullout behavior of inclined deformed steel fibers embedded in ultra-high performance concrete, Constr. Build. Mater. 148 (2017) 204-218.

[25] F. Dai, K. Xia, H. Zheng, and Y. X. Wang, Determination of dynamic rock Mode-I fracture parameters using cracked chevron notched semi-circular bend specimen, Eng. Fract. Mech. 78(15) (2011) 2633-2644.

[26] A. a. A. Molenaar, A. Scarpas, X. Liu, and S. M. J. G. Erkens, "Semi-circular bending test; simple but useful?, Journal of the Association of Asphalt Paving Technologists, 71 (2002).

[27] M. R. Ayatollahi and M. R. M. Aliha, Fracture toughness study for a brittle rock subjected to mixed mode I/II loading, Int. J. Rock Mech. Min. Sci. 44(4) (2007) 617-624.

[28] I. L. Lim, I. W. Johnston, S. K. Choi, and J. N. Boland, "Fracture testing of a soft rock with semi-circular specimens under three-point bending. Part 1—mode I," Int. J. Rock Mech. Min. Sci. Geomech. Abstr., vol. 31, no. 3, pp. 185–197, Jun. 1994.

[29] I. L. Lim, I. W. Johnston, S. K. Choi, and J. N. Boland, Fracture testing of a soft rock with semi-circular specimens under three-point bending. Part 2—mixed-mode, Int. J. Rock Mech. Min. Sci. Geomech. Abstr. 31(3) (1994) 199-212.

[30] M. Arabani and B. Ferdowsi, "Evaluating the semi-circular bending test for HMA mixtures," Int. J. Eng. Trans. Basics. 22(1) (2008).

[31] F. Dai, R. Chen, and K. Xia, A Semi-Circular Bend Technique for Determining Dynamic Fracture Toughness, Exp. Mech. 50(6) (2009) 783-791.

[32] M. R. Ayatollahi, M. R. M. Aliha, and H. Saghafi, An improved semi-circular bend specimen for investigating mixed mode brittle fracture, Eng. Fract. Mech. 78(1) (2011) 110-123.

[33] G. Nsengiyumva, Development of Semi-Circular Bending (SCB) Fracture Test for Bituminous Mixtures, Civ. Eng. Theses Diss. Stud. Res. (2015)

[34] S. Tang, Evaluate the fracture and fatigue resistances of hot mix asphalt containing high percentage reclaimed asphalt pavement (RAP) materials at low and intermediate temperatures, Grad. Theses Diss. (2014).

[35] I. M. Lancaster, H. A. Khalid, and I. A. Kougioumtzoglou, Extended FEM modelling of crack propagation using the semi-circular bending test, Constr. Build. Mater. 48 (2013) 270-277.

[36] E. Mahmoud, S. Saadeh, H. Hakimelahi, and J. Harvey, Extended finite-element modelling of asphalt mixtures fracture properties using the semi-circular bending test, Road Mater. Pavement Des. 15(1) (2014) 153-166.

[37] B.S.1881-116; 1983. Testing Concrete. Method for determination of Compressive Strength of Concrete cubes. British Standards Institute. London, United Kingdom.

[38] M. T. Kazemi, H. Golsorkhtabar, M. H. A. Beygi, and M. Gholamitabar, Fracture properties of steel fiber reinforced high strength concrete using work of fracture and size effect methods, Constr. Build. Mater. 142 (2017) 482-489.

[39] A. Emdadi, I. Mehdipour, N. A. Libre, and M. Shekarchi, Optimized workability and mechanical properties of FRCM by using fiber factor approach: theoretical and experimental study, Mater. Struct. 48(4) (2015) 1149-1161.

[40] I. Mehdipour and N. A. Libre, Linking Fiber Factor to Material Performance of Fiber-Reinforced Self-Consolidating Cement-Based Materials, ACI Mater. J. 114(1) (2017).

[41] M. T. Kazemi, H. Golsorkhtabar, M. H. A. Beygi, and M. Gholamitabar, Fracture properties of steel fiber reinforced high strength concrete using work of fracture and size effect methods, Constr. Build. Mater. 142 (2017) 482-489.

[42] M. Chellapandian, S. Suriya Prakash, and A. Sharma, Strength and ductility of innovative hybrid NSM reinforced and FRP confined short RC columns under axial compression, Compos. Struct. 176 (2017) 205-216.

[43] ASTM C1609 / C1609M-12, Standard Test Method for Flexural Performance of Fiber-Reinforced Concrete (Using Beam With Third-Point Loading), ASTM International, West Conshohocken, PA, 2012.

[44] ASTM C1609 / C1609M-12, Standard Test Method for Flexural Performance of Fiber-Reinforced Concrete (Using Beam With Third-Point Loading), ASTM International, West Conshohocken, PA, 2012.

[45] U. N. Gokoz and A. E. Naaman, Effect of strain-rate on the pull-out behaviour of fibres in mortar, Int. J. Cem. Compos. Lightweight Concr. 3(3) (1981) 187-202.

[46] A. Khabaz, Analysis of sliding mechanism of straight steel fibers in concrete and determine the effect of friction, Arch. Civ. Mech. Eng. 17(3) (2017) 599-608.

[47] N. T. Tran, T. K. Tran, J. K. Jeon, J. K. Park, and D. J. Kim, Fracture energy of ultra-high-performance fiber-reinforced concrete at high strain rates, Cem. Concr. Res. 79 (2016) 169-184.

[48] N. Banthia, A study of some factors affecting the fiber–matrix bond in steel fiber reinforced concrete, Can. J. Civ. Eng. 17 (1990) 610-620.

[49] N. Banthia and J.-F. Trottier, Deformed steel fiber cementitious matrix bond under impact, Cem. Concr. Res. 21(1) (1991) 158-168.

List of Tables

List of Figures

Figure 17 Force-Displacement diagram of steel fiber reinforced concrete at 0.5, 1, and 5 m/sec loading rates

Figure 18 Peak loads for all FRC samples at three loading rate

Figure 19 Area under curves for all FRC samples at three loading rate

Figure 20 Ratio of peak loads for all FRC samples at three loading rat

Table 1
Click here to download Table: Table 1.docx

Table.1 Chemical composition of cement and silica fume

Items	Cement (%)	Silica fume (%)
SiO_2	20.38	85.19
Al_2O_3	4.13	0.31
Fe_2O_3	3.82	3.42
CaO	62.96	0.75
MgO	3.5	2.06
SO_3	2.87	–
LOI	0.98	3.8

Table 2
Click here to download Table: Table 2.docx

Table 2. Specification of glass, polypropylene and steel fibers

Fiber type	Length (mm)	Diameter (µm)	Shape	Specific gravity (kg/m^3)	Tensile strength (MPa)	Modulus of elasticity (MPa)
Steel (ST)	12.5	180	Plain	7800	1400	200000
Polypropylene (PP)	12.5	19	Plain	910	450	5000
Glass (G)	12.5	17	Plain	2580	3445	72300

Table 3

Table 3 . Fracture parameters of control and fiber reinforced concrete samples

Sample Code	Peak Load (N)	Displacement at Peak (mm)	Maximum Displacement (mm)	Second Peak Load (N)
Control	2007.0	0.2516	0.2575	0.0
G 0.5%	2579.6	0.3475	5.6781	762.6
G 1.0%	2611.1	0.5133	9.2521	1762.5
G 1.5%	3088.9	0.6026	12.060	2256.2
PP 0.5%	2487.7	0.4791	5.7606	462.31
PP 1.0%	2358.7	0.5658	8.5496	943.2
PP 1.5%	2636.9	0.5749	8.5763	1327.2
ST 0.5%	2173.66	0.5916	6.2905	1175.9
ST 1.0%	3000.75	0.5000	6.2497	1867.9
ST 1.5%	3528.46	0.3650	5.9864	3517.2

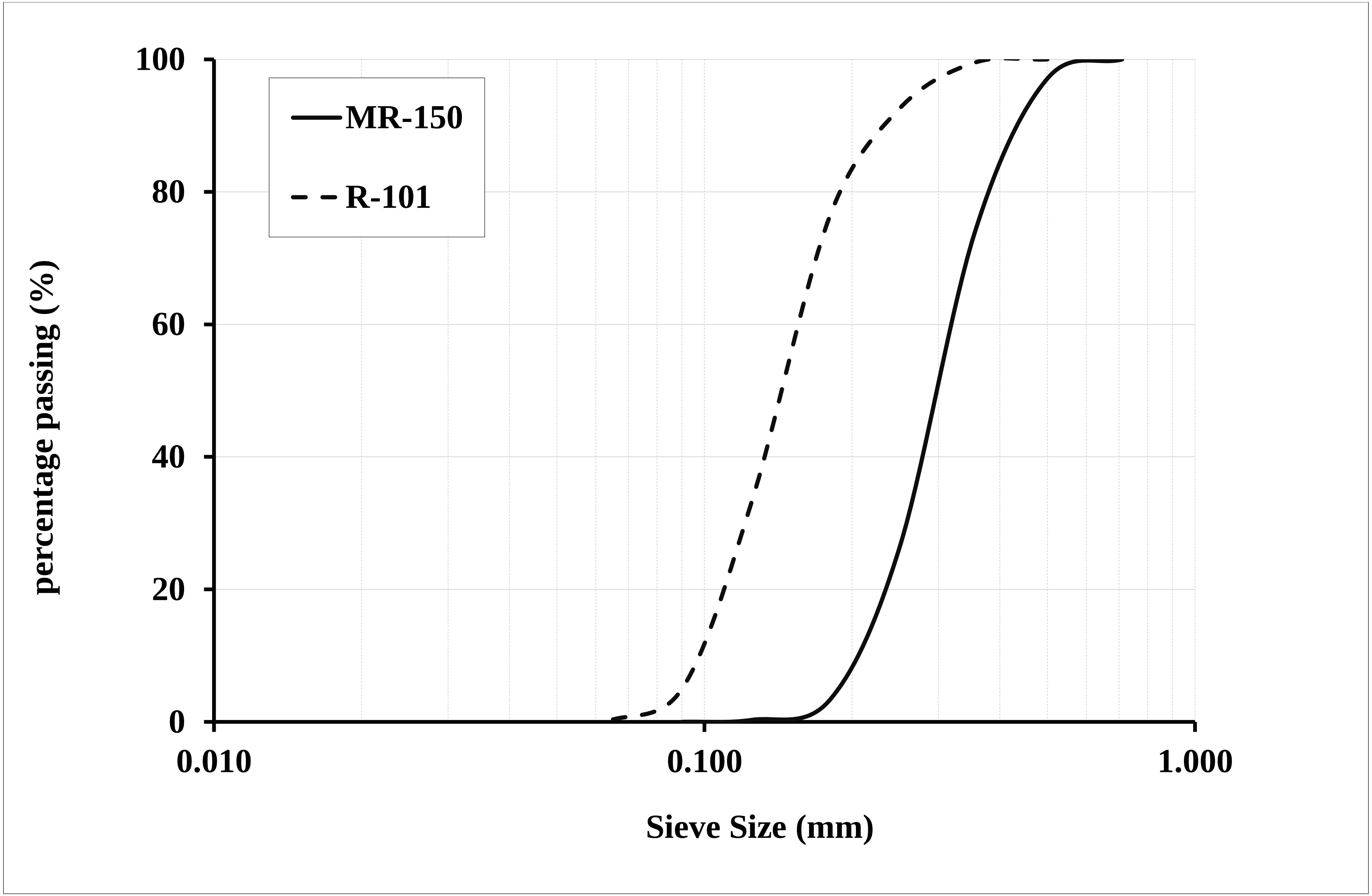
MR-150
R-101
100
80
60
40
20
0
percentage passing (%)
0.010
0.100
1.000
Sieve Size (mm)

figure 10.pdf
Click here to download Figure: Figure 10.pdf

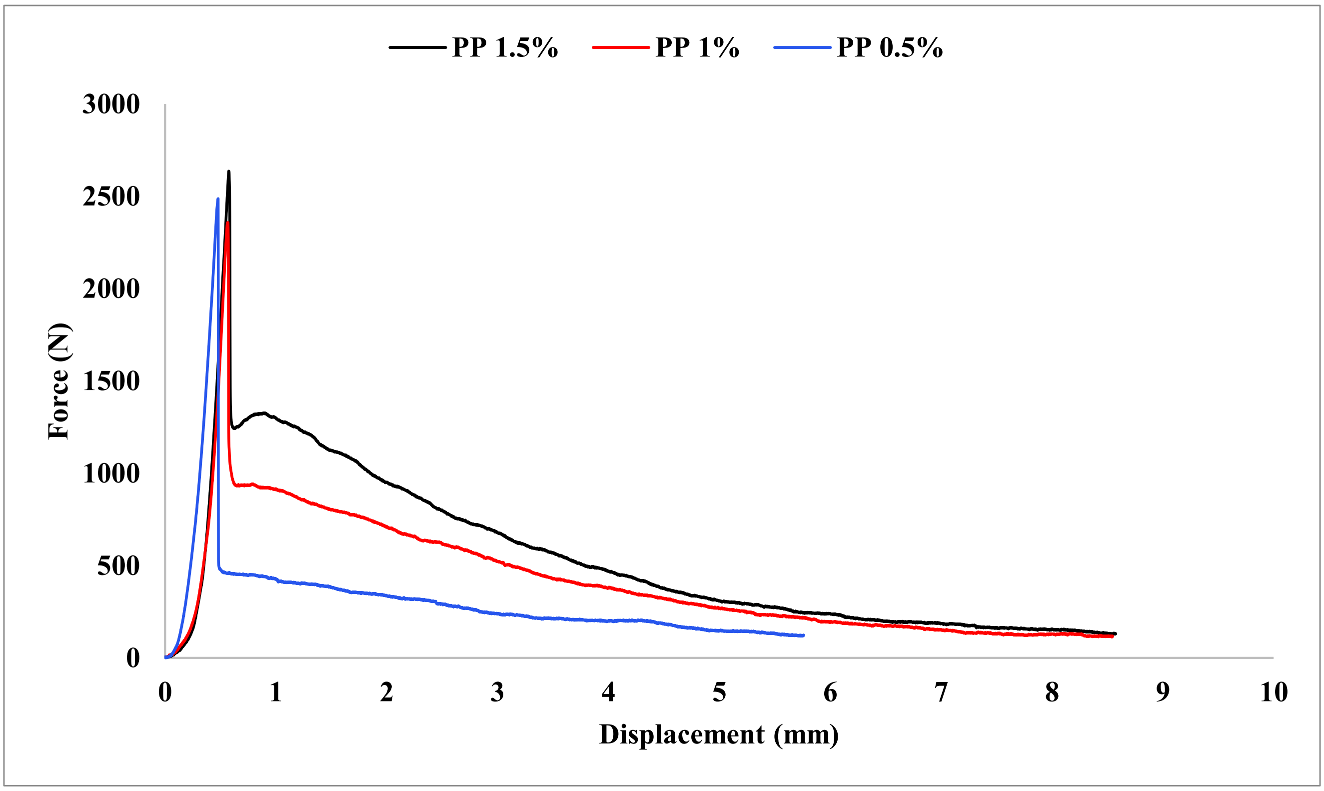

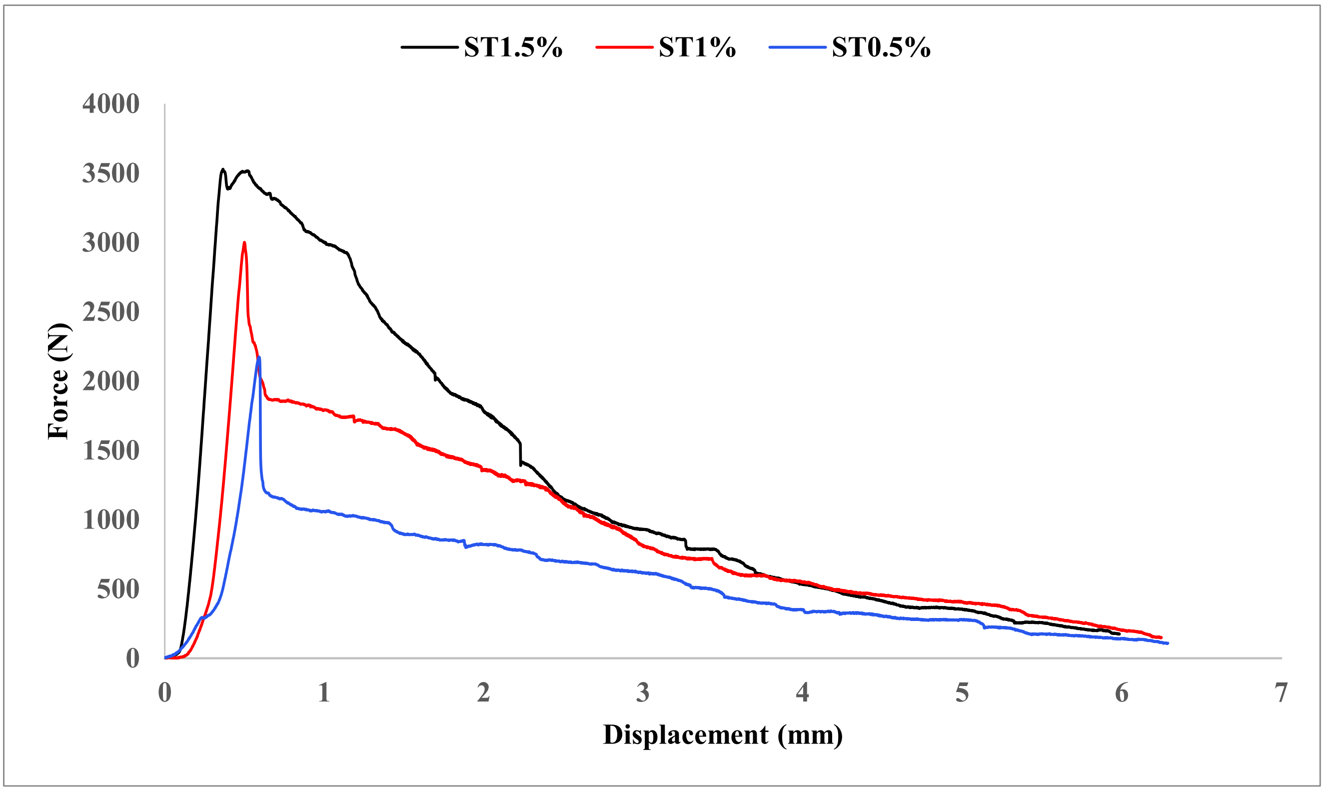
ST1.5%
ST1%
ST0.5%
4000
3500
3000
2500
2000
1500
1000
500
0
Force (N)
0
1
2
3
4
5
6
7
Displacement (mm)

figure 12.pdf
Click here to download Figure: Figure 12.pdf

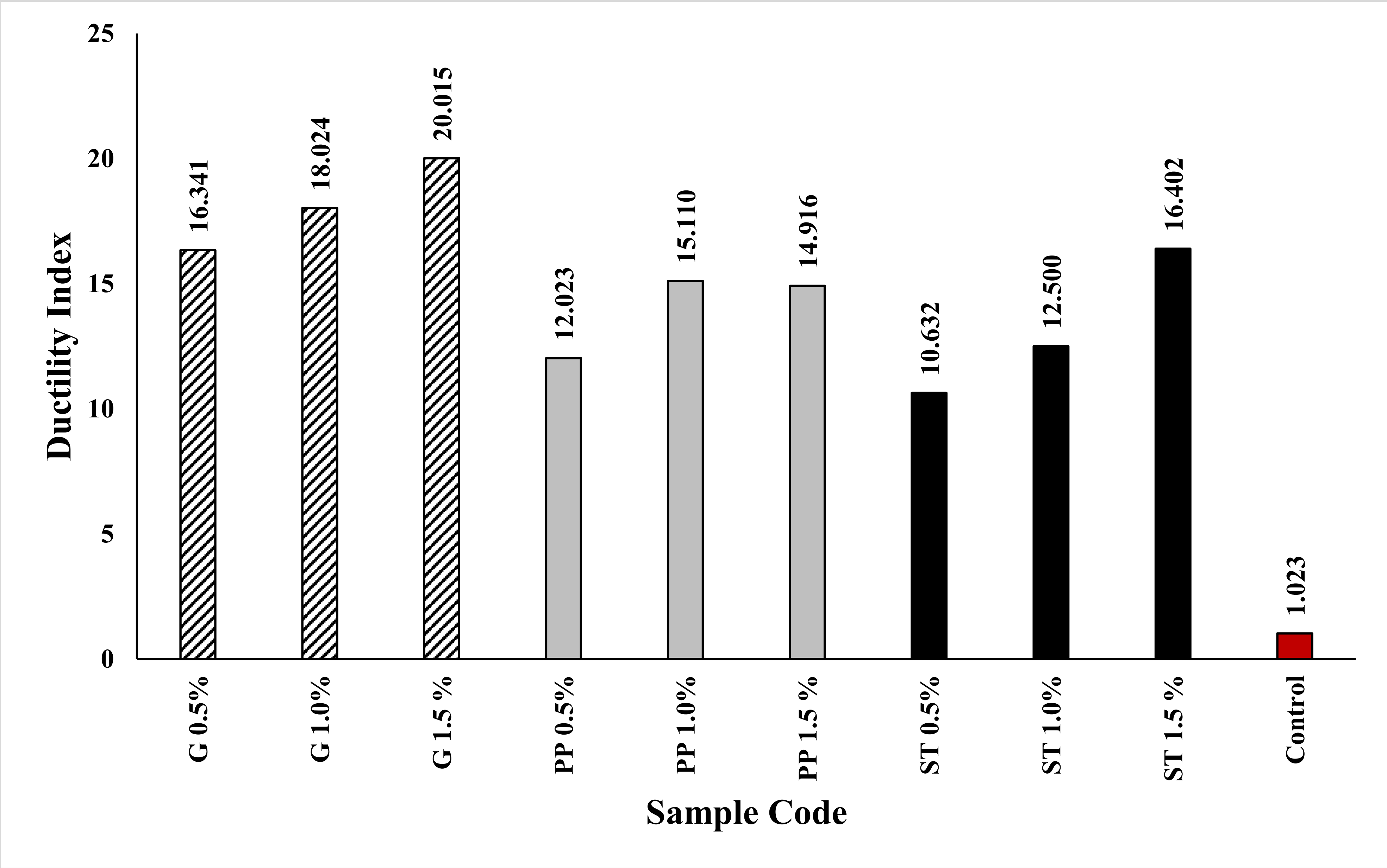

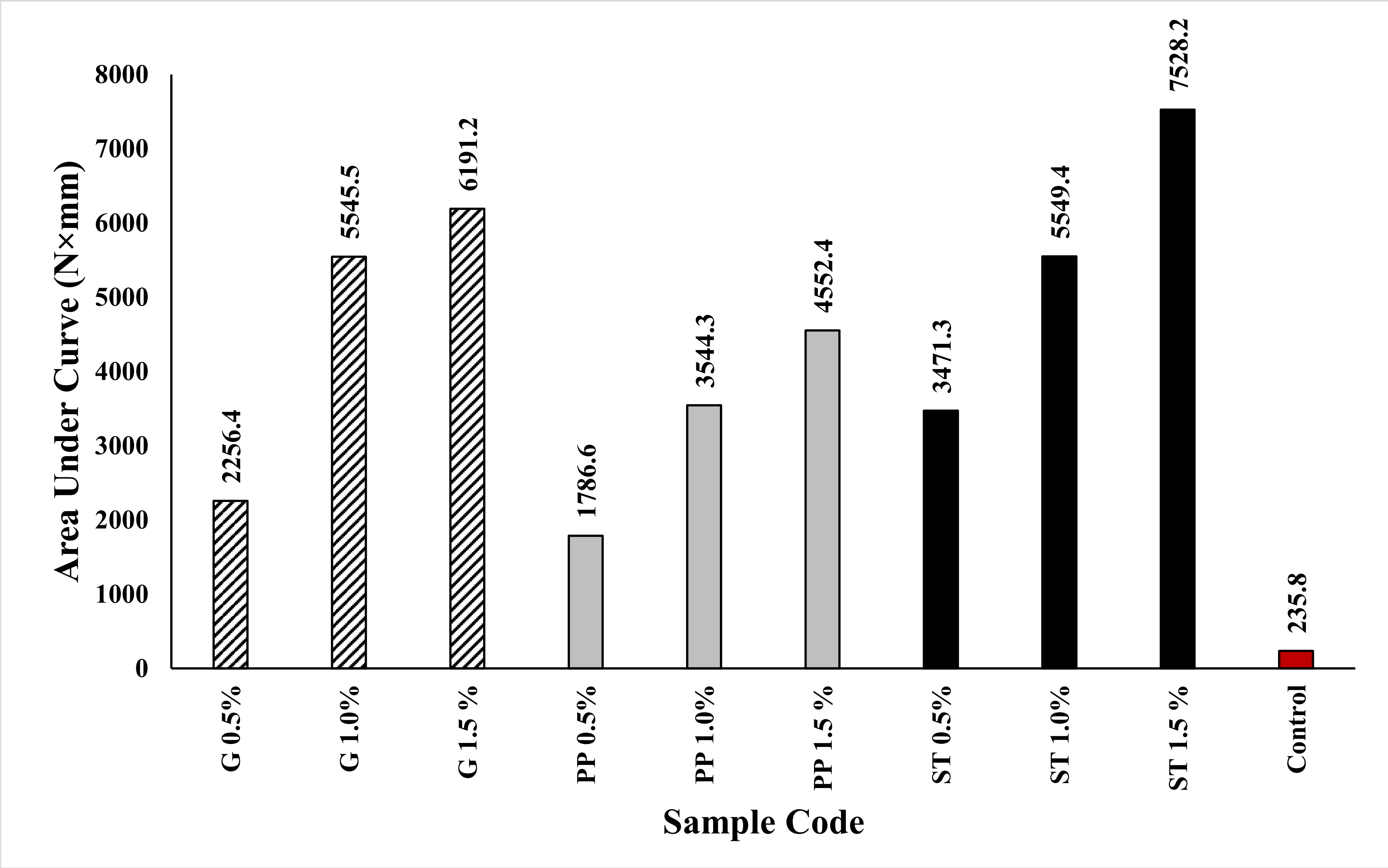
Area Under Curve (N×mm)
8000
7000
6000
5000
4000
3000
2000
1000
0
2256.4
5545.5
6191.2
1786.6
3544.3
4552.4
3471.3
5549.4
7528.2
235.8
G 0.5%
G 1.0%
G 1.5 %
PP 0.5%
PP 1.0%
PP 1.5 %
ST 0.5%
ST 1.0%
ST 1.5 %
Control
Sample Code

figure 14.pdf
Click here to download Figure: Figure 14.pdf

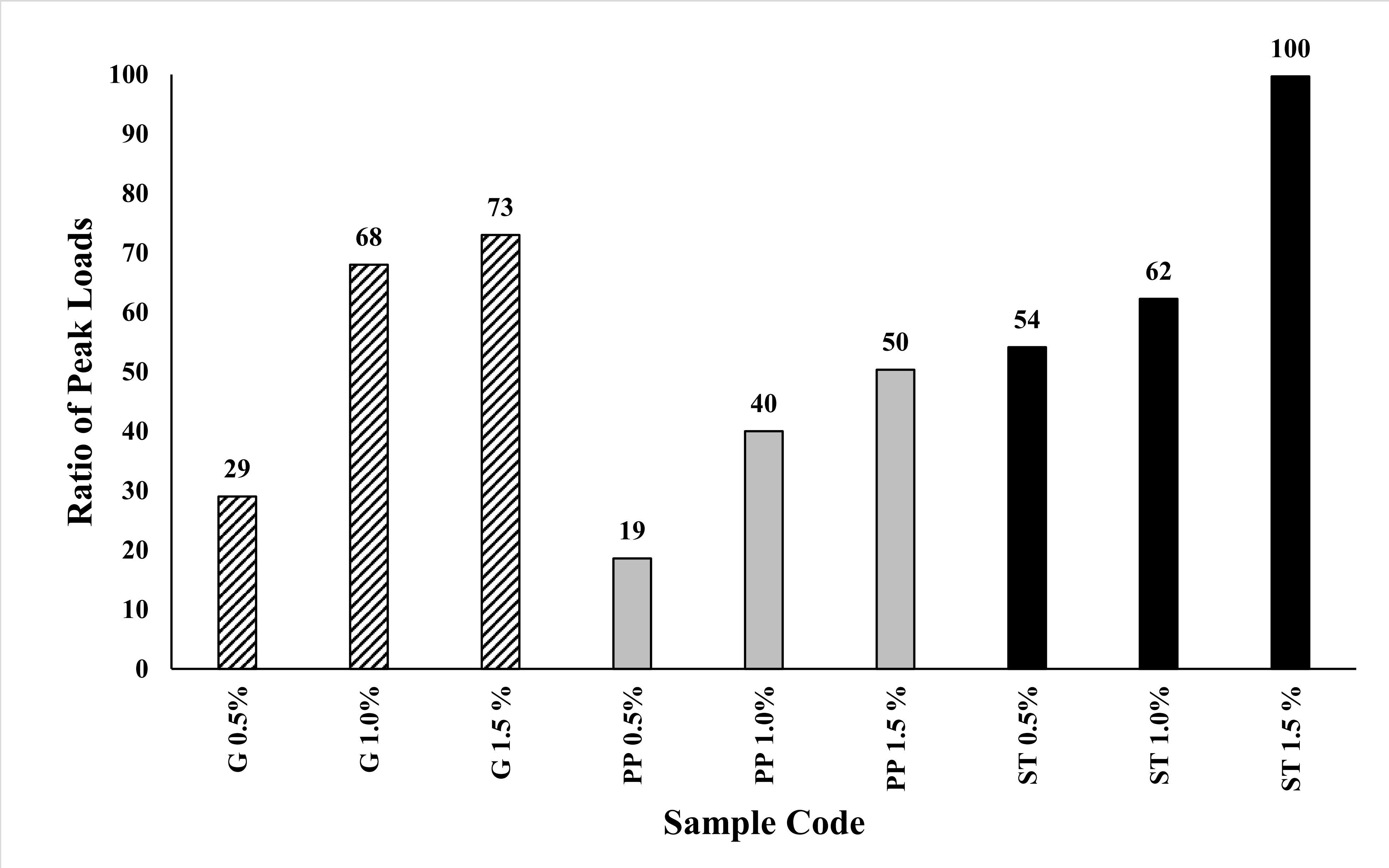

figure 15.pdf
Click here to download Figure: Figure 15.pdf

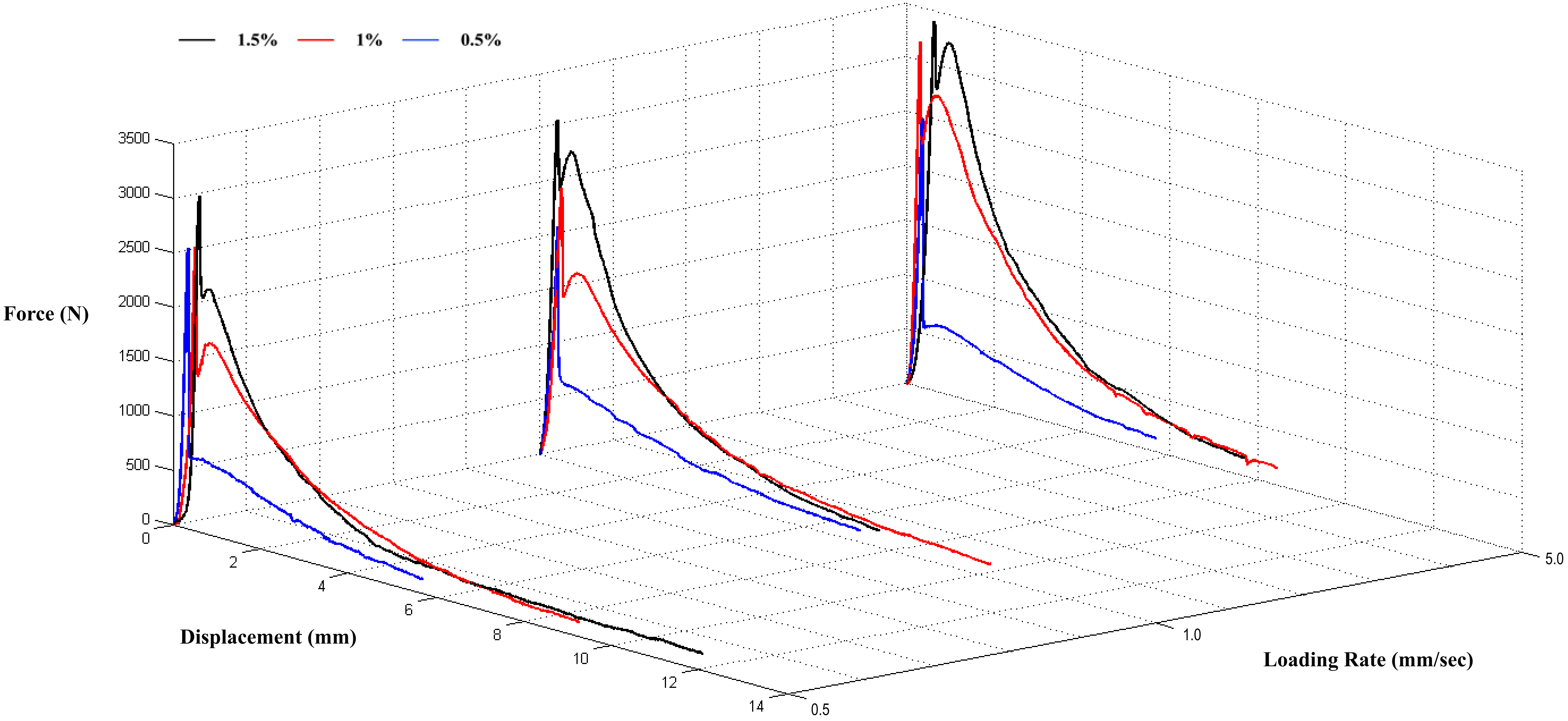

figure 16.pdf
Click here to download Figure: Figure 16.pdf

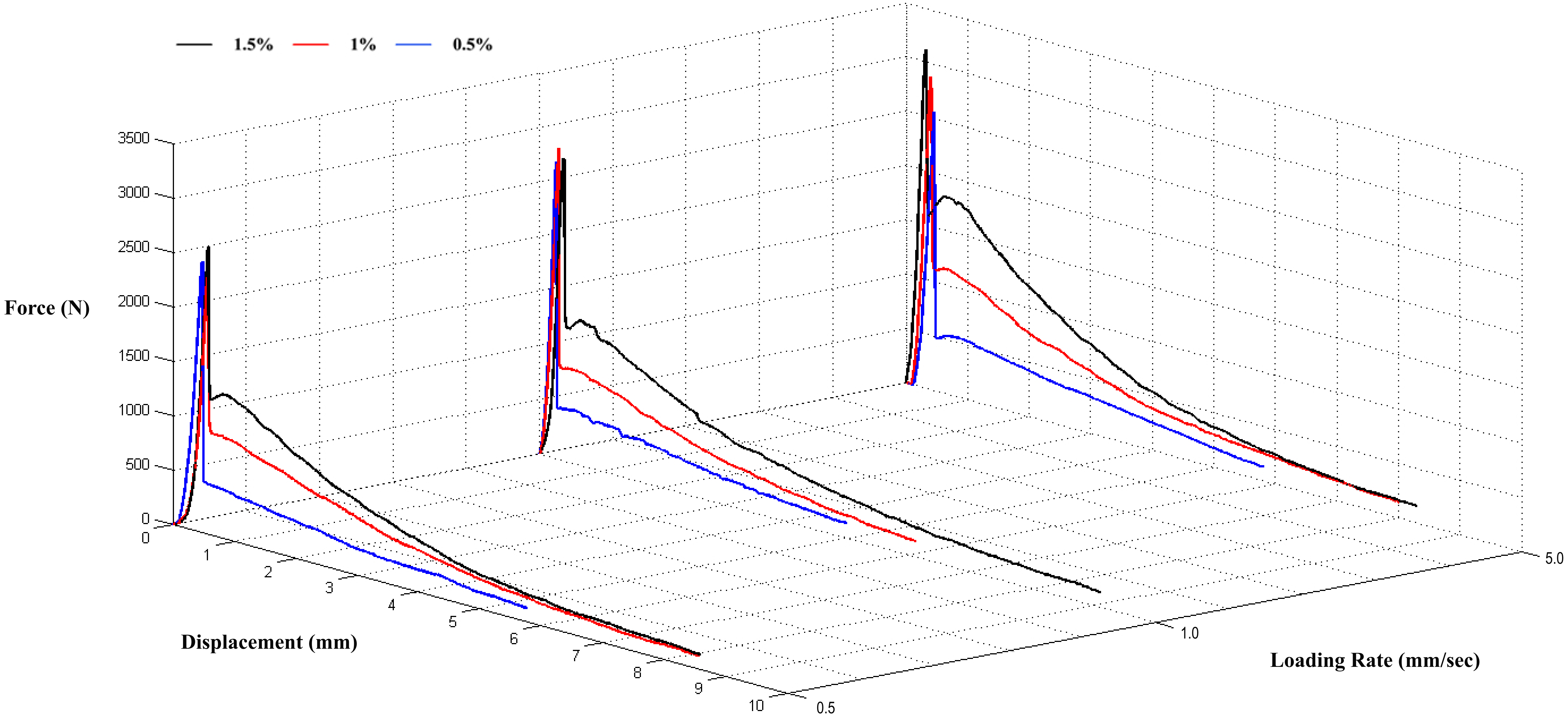

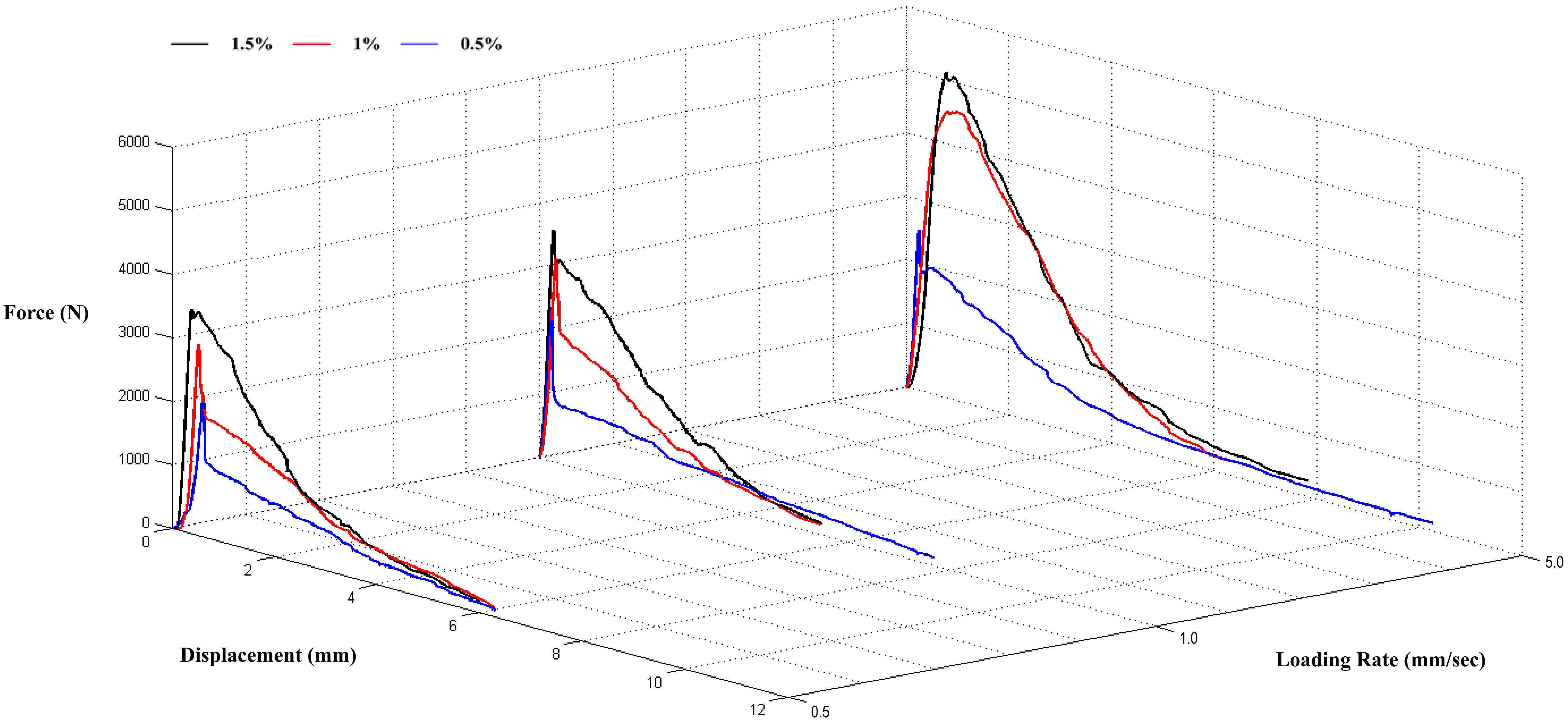
1.5%
1%
0.5%
Force (N)
6000
5000
4000
3000
2000
1000
0
0
2
4
6
8
10
12
Displacement (mm)
0.5
1.0
5.0
Loading Rate (mm/sec)

figure 18.pdf
Click here to download Figure: Figure 18.pdf

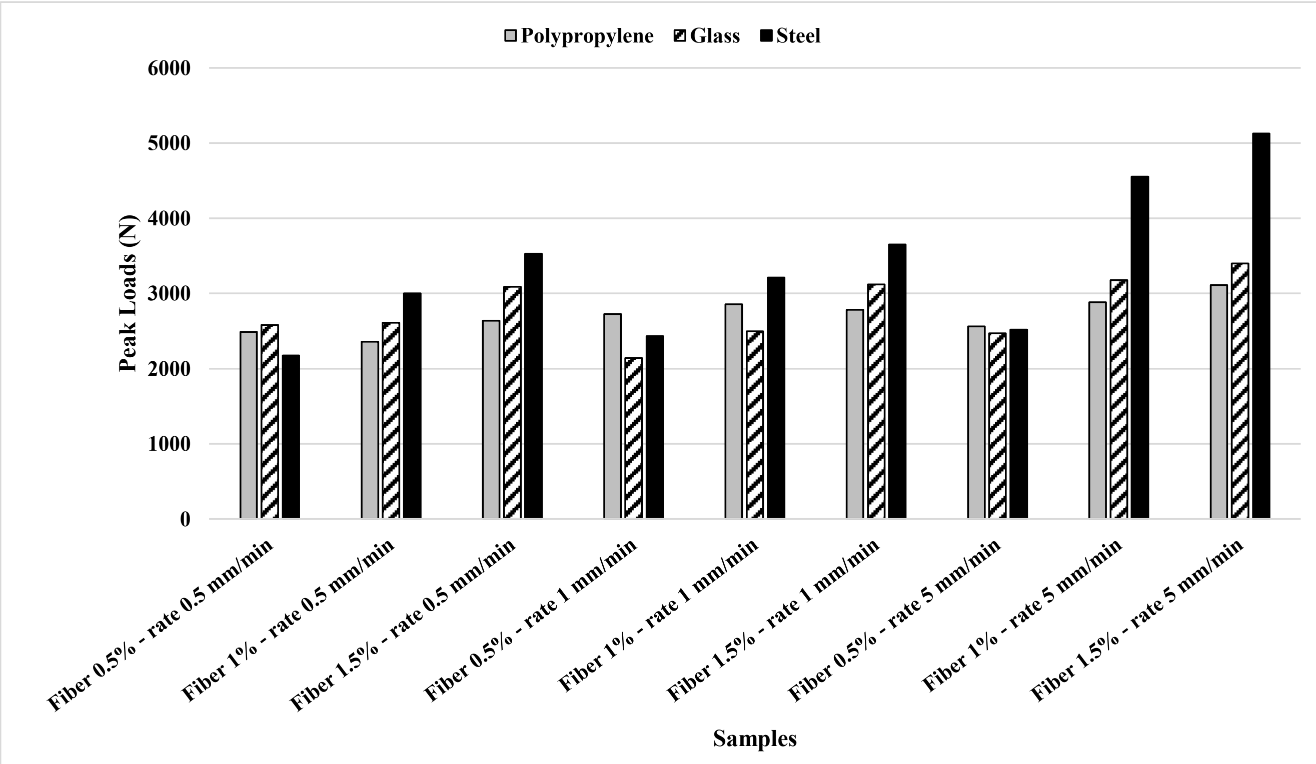

figure 19.pdf
Click here to download Figure: Figure 19.pdf

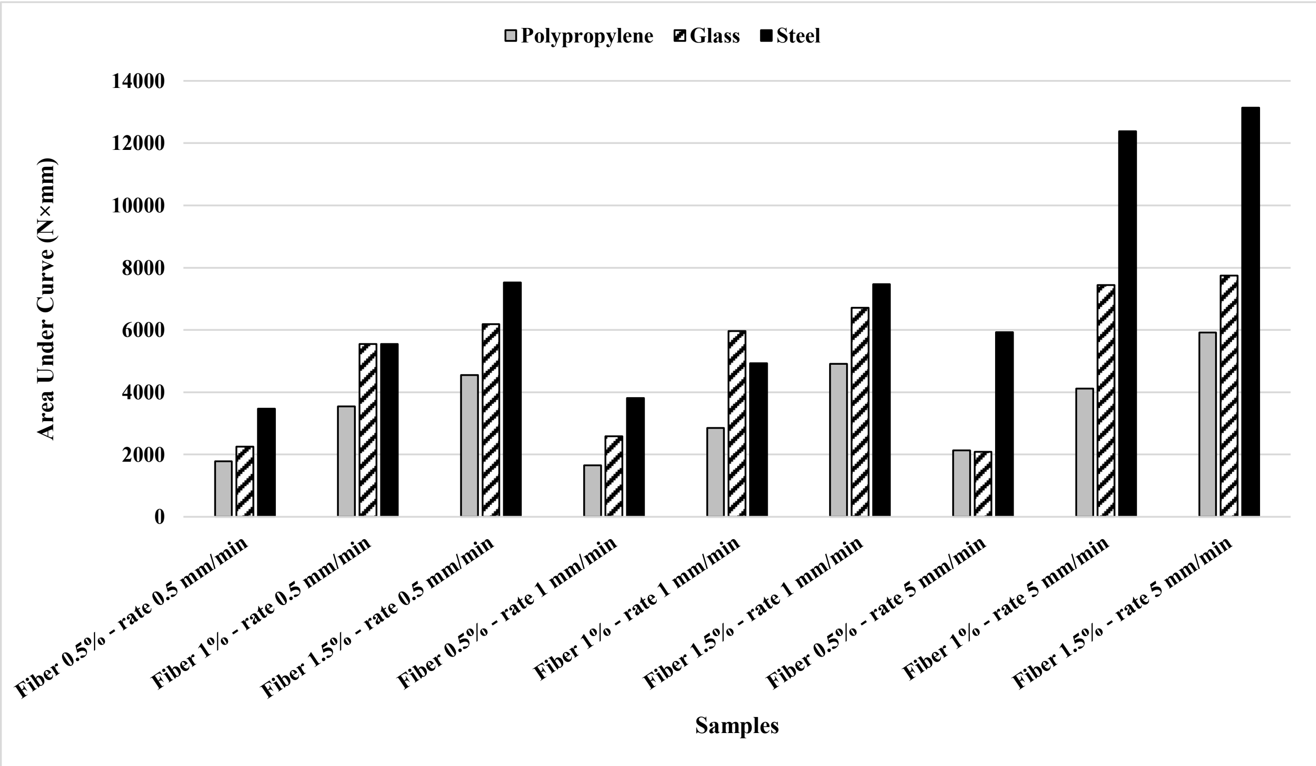


Polypropylene
Steel
Glass
12.5 mm

figure 20.pdf
Click here to download Figure: Figure 20.pdf

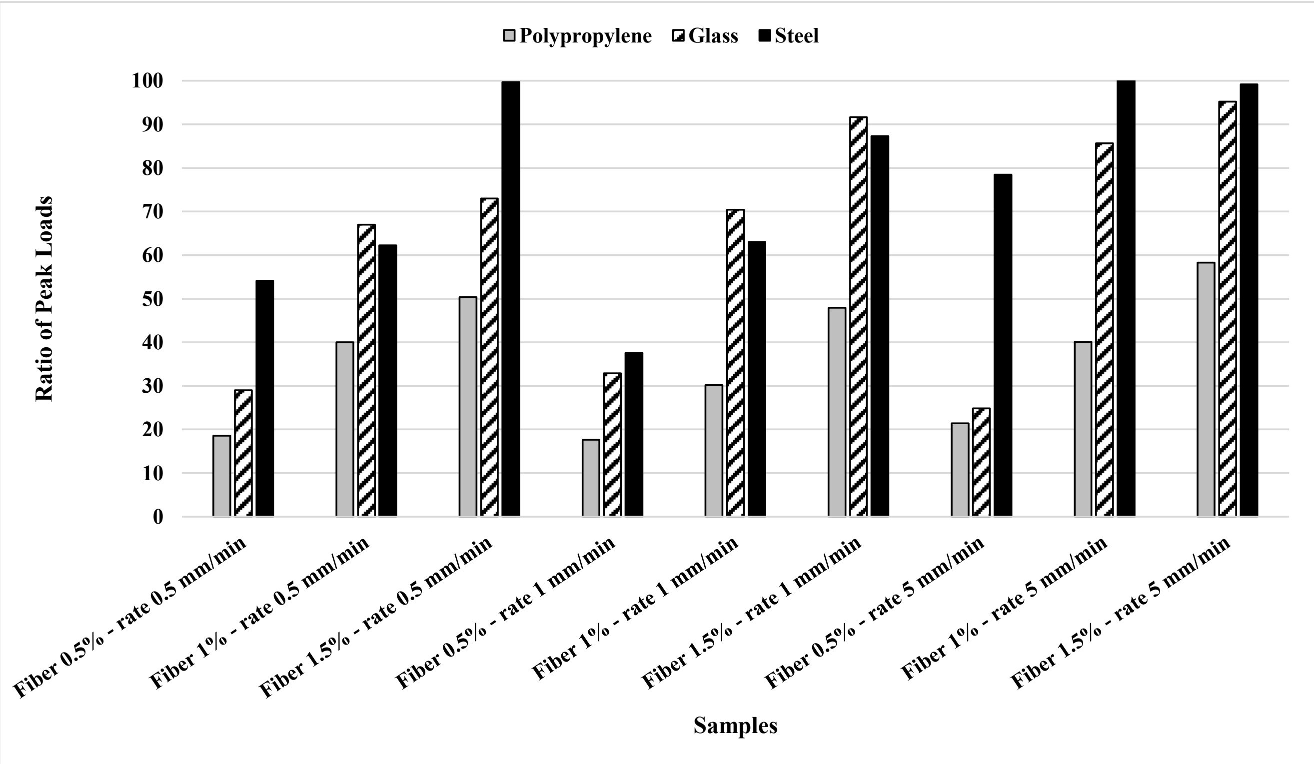

figure 3-a.pdf
Click here to download Figure: Figure 3-a.pdf

figure 3-b.pdf

Click here to download Figure: Figure 3-b.pdf

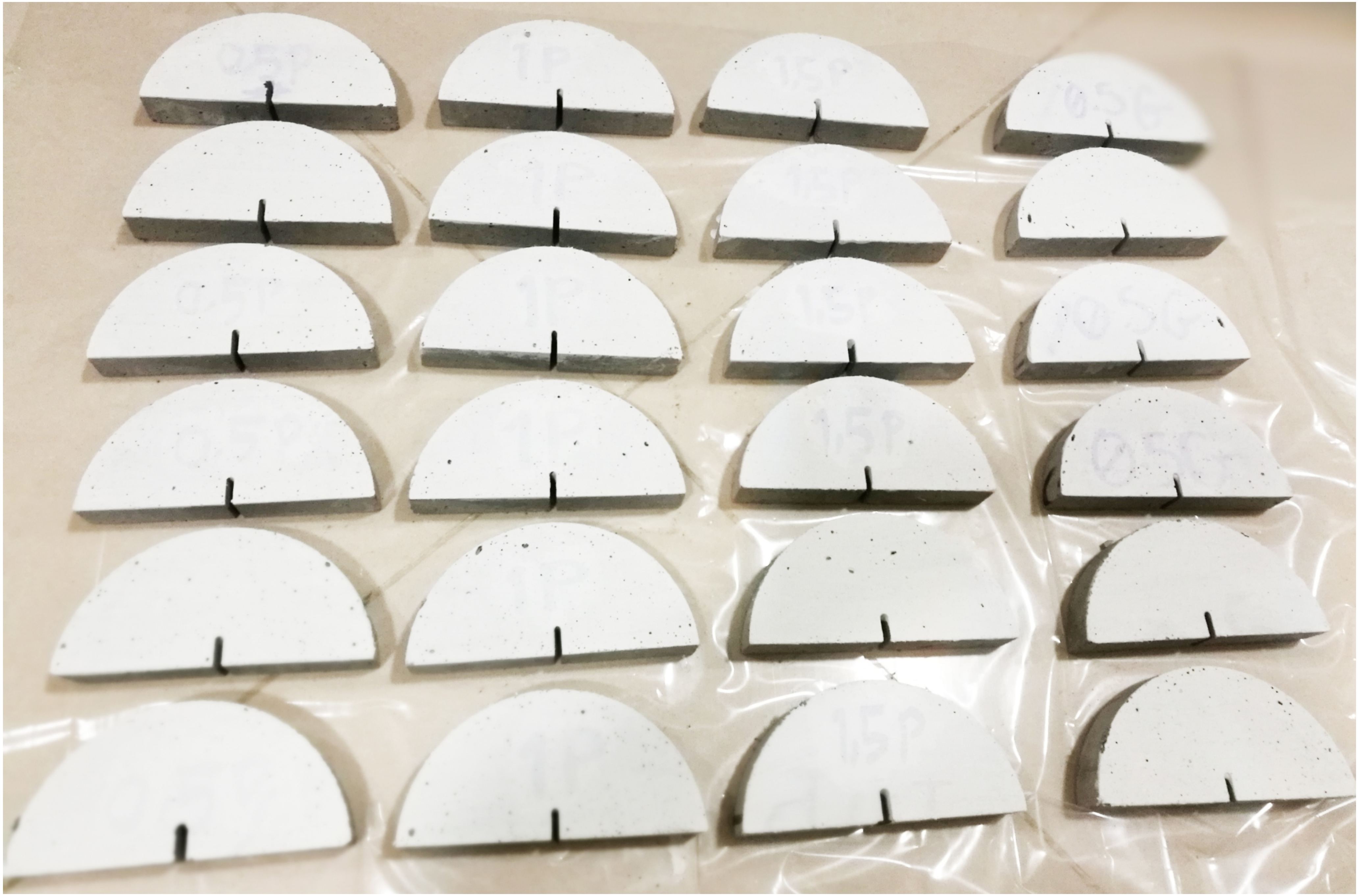

figure 4.pdf

[Click here to download Figure: Figure 4.pdf]

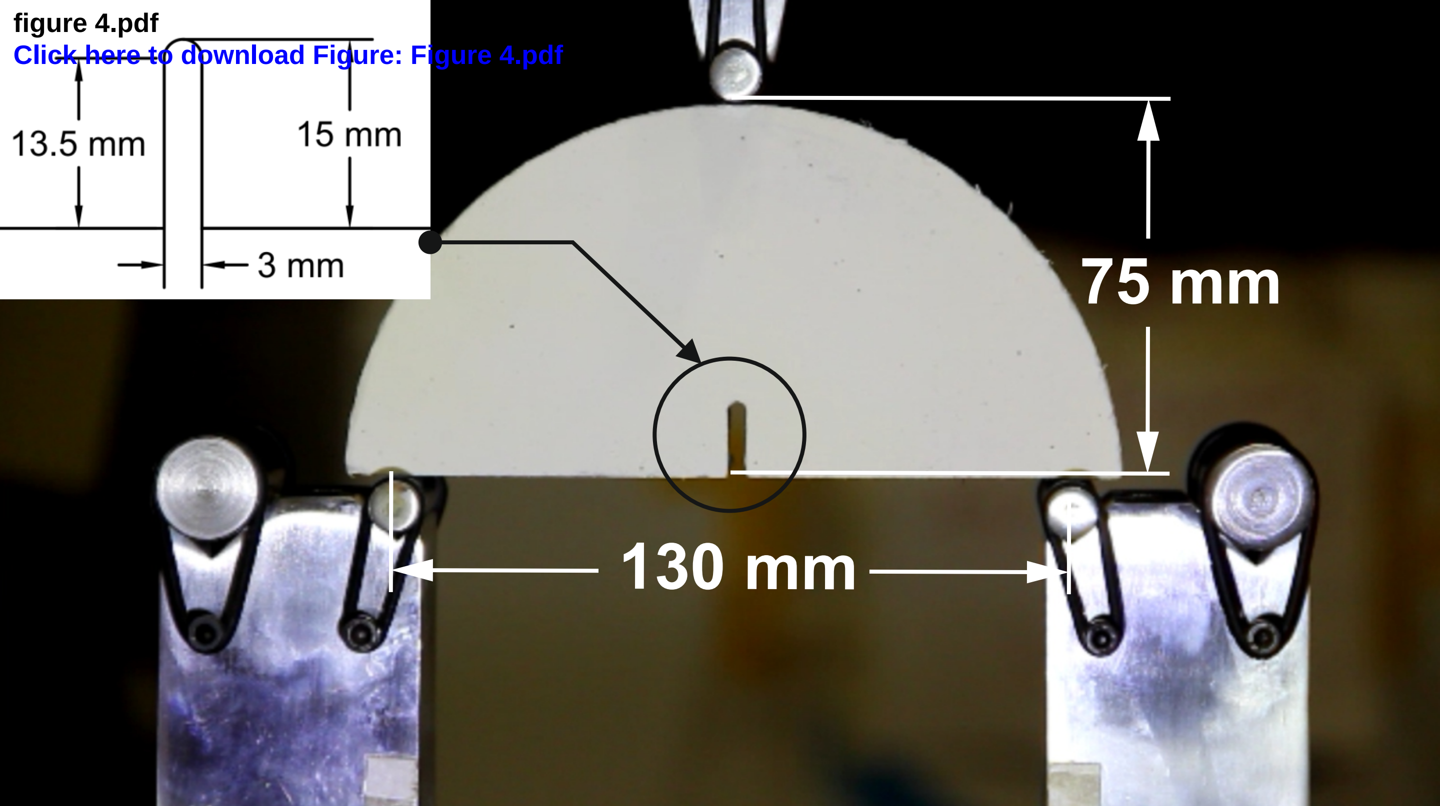

figure 5.pdf
Click here to download Figure: Figure 5.pdf

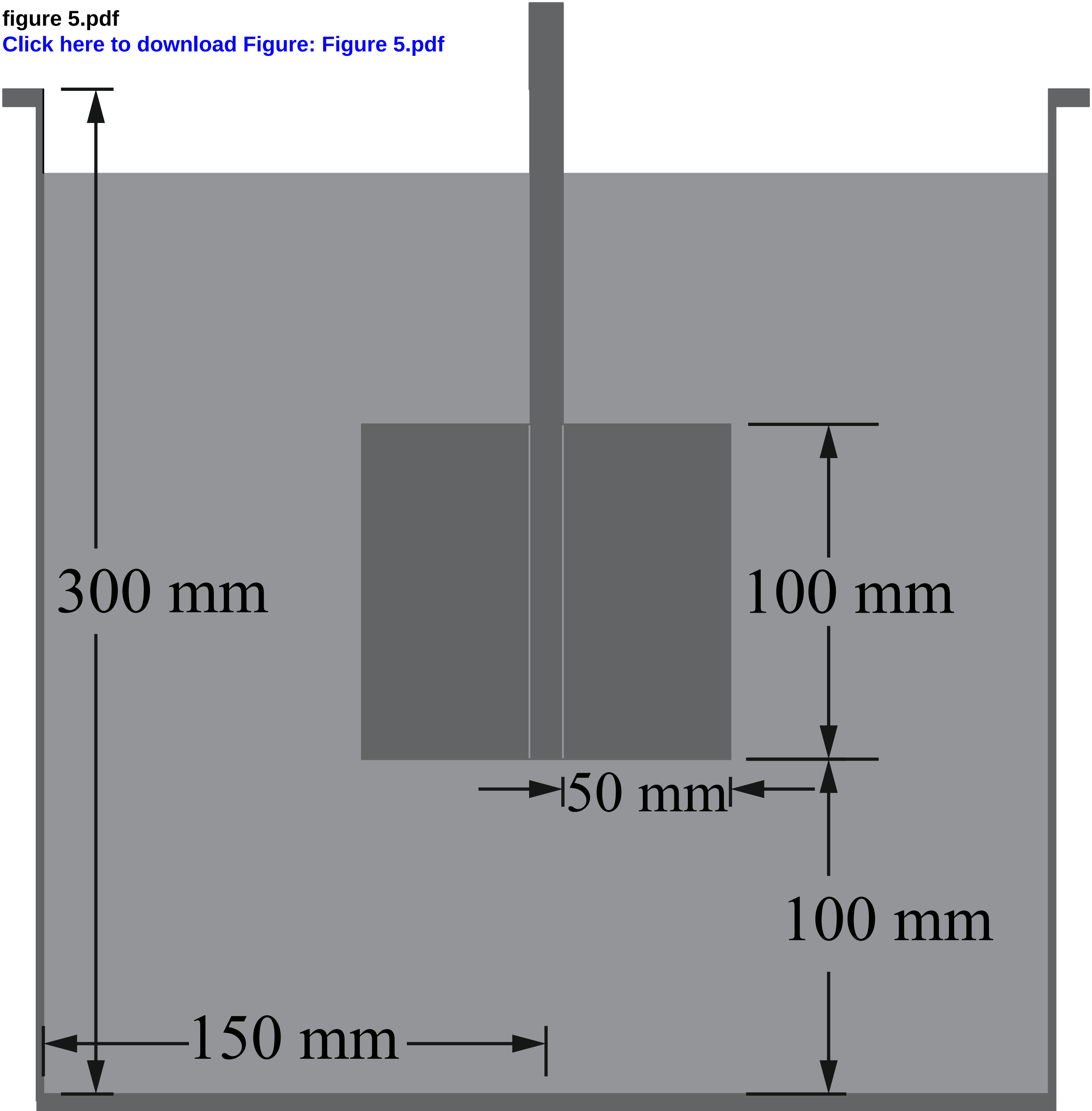

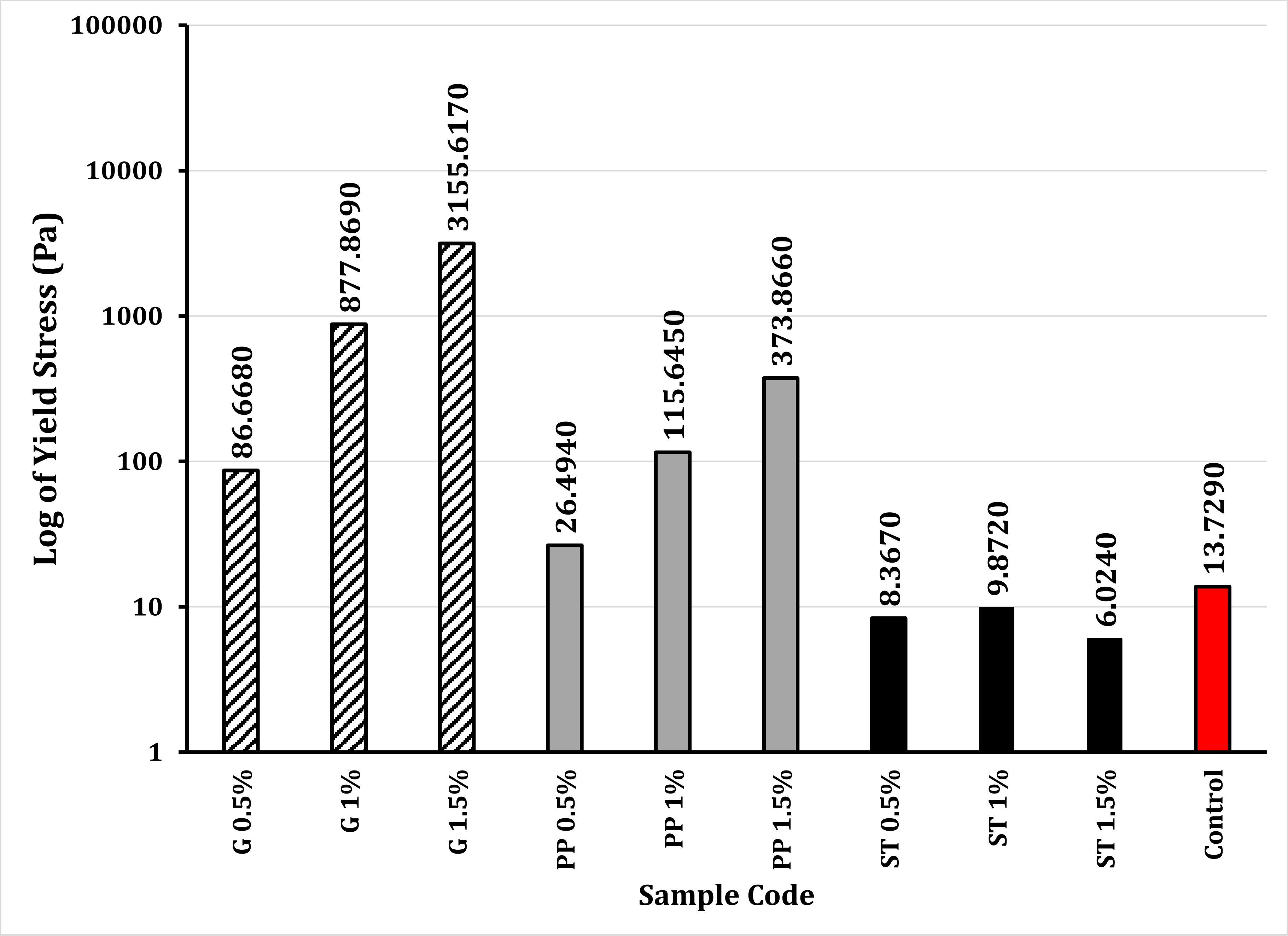
100000
10000
1000
100
10
1
Log of Yield Stress (Pa)
86.6680
877.8690
3155.6170
26.4940
115.6450
373.8660
8.3670
9.8720
6.0240
13.7290
G 0.5%
G 1%
G 1.5%
PP 0.5%
PP 1%
PP 1.5%
ST 0.5%
ST 1%
ST 1.5%
Control
Sample Code

figure 7.pdf
Click here to download Figure: Figure 7.pdf

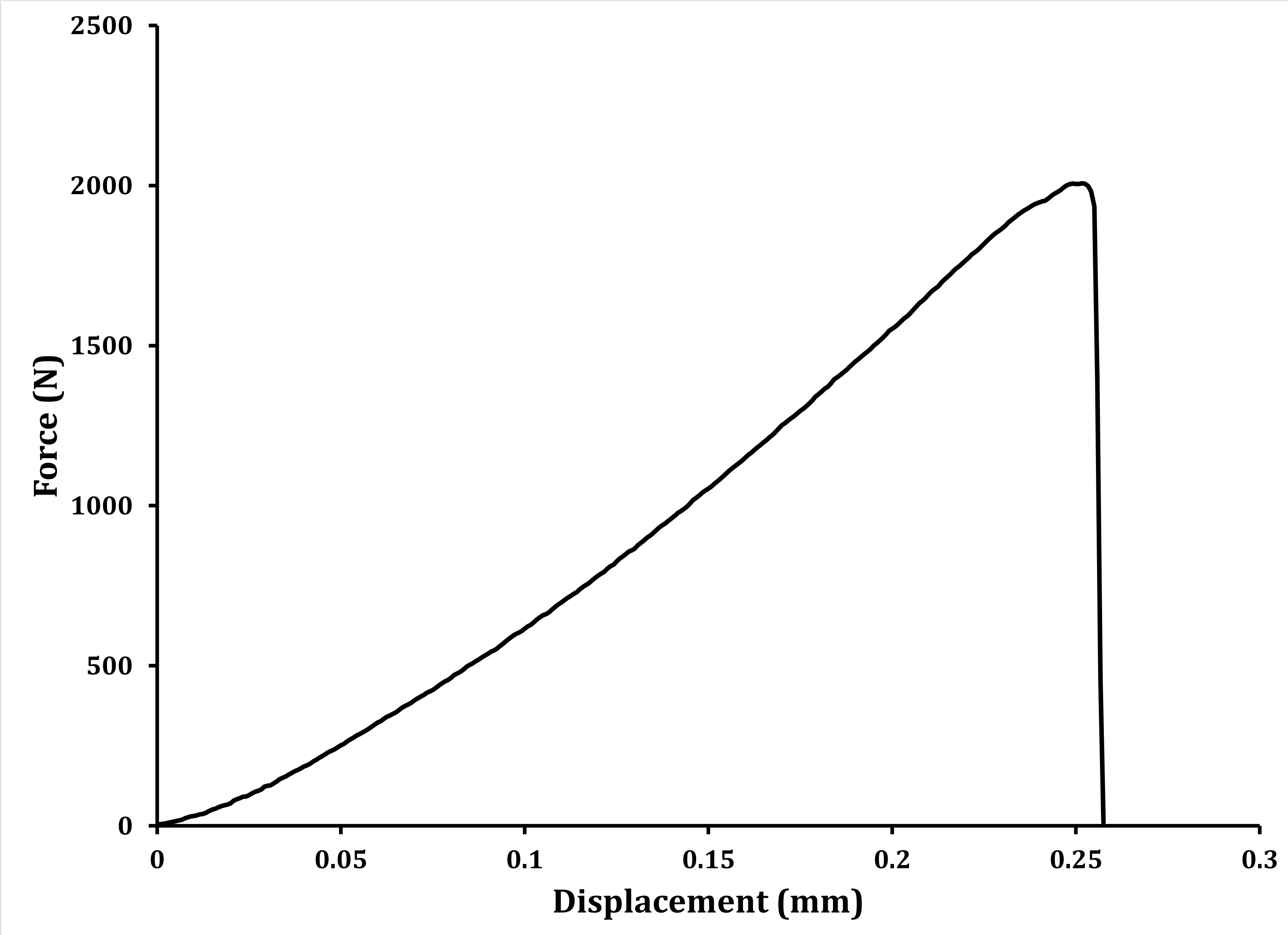

figure 8-a.pdf
Click here to download Figure: Figure 8-a.pdf

figure 8-b.pdf
Click here to download Figure: Figure 8-b.pdf

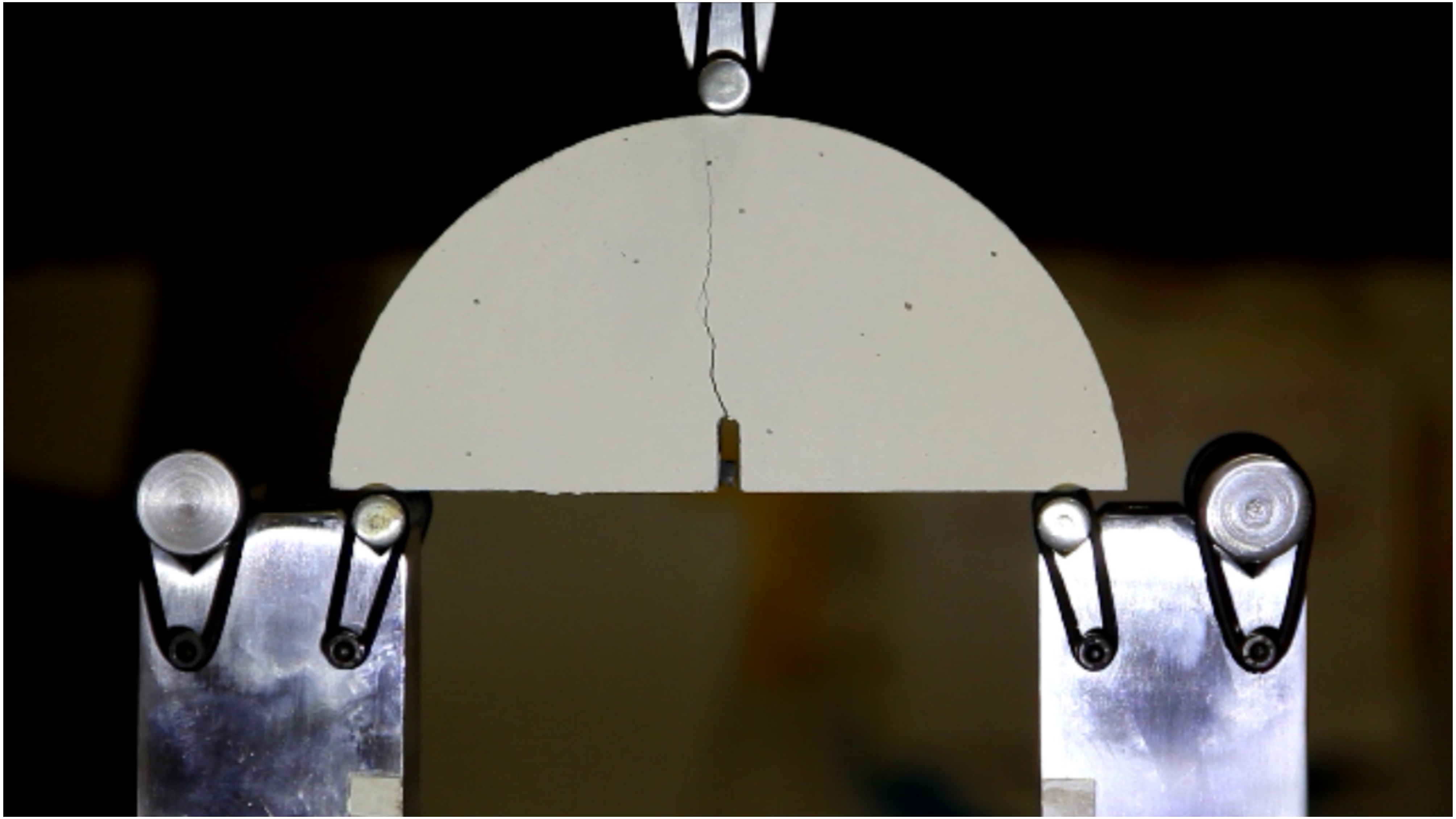

figure 8-c.pdf
Click here to download Figure: Figure 8-c.pdf

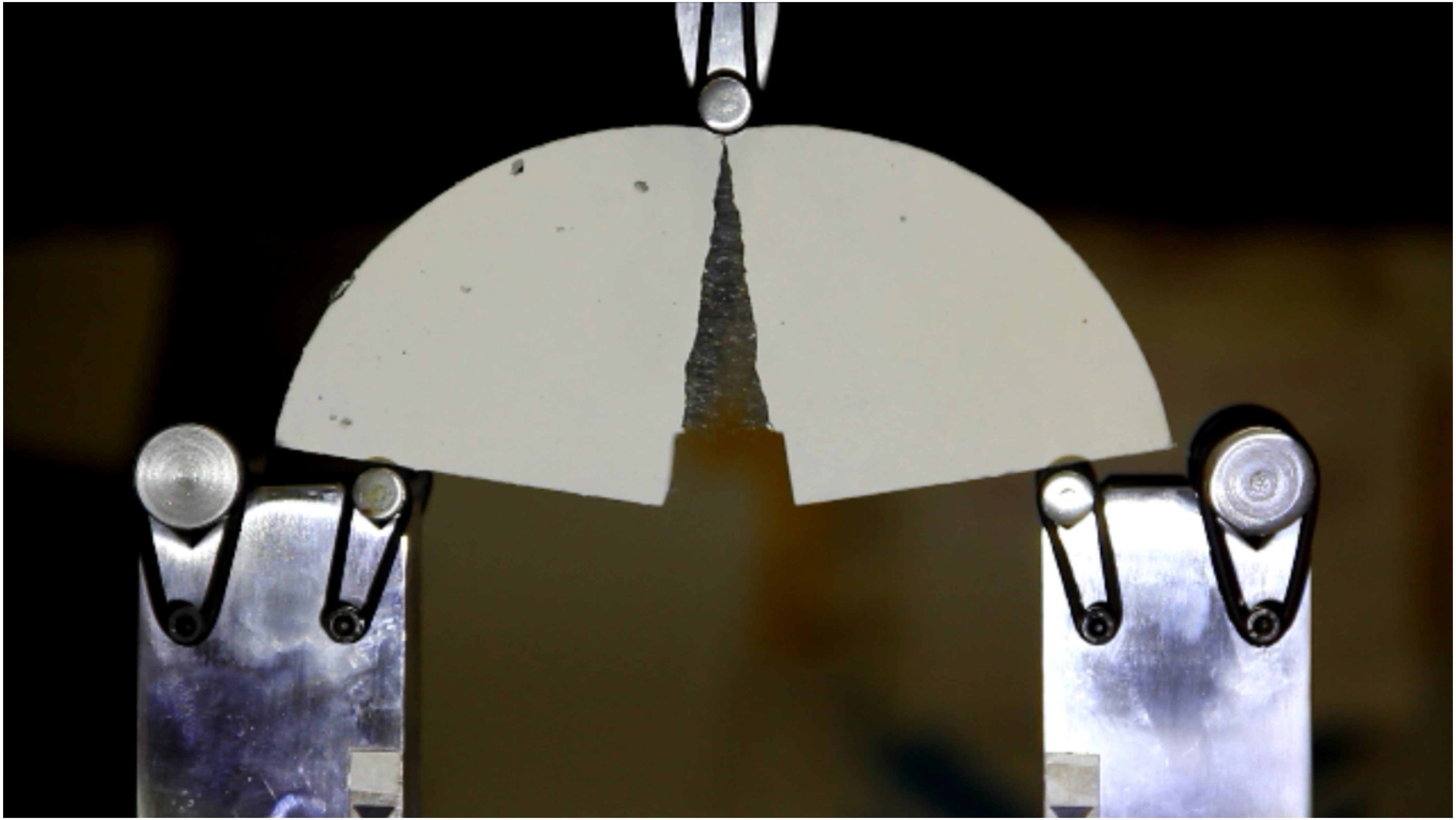

figure 9.pdf
Click here to download Figure: Figure 9.pdf